Electronic Supplementary Information

Reversible anion-dependent iodine uptake in nonporous pseudopolymorphic coordination polymers

Ghazale Khorshidi,[a] Behrouz Notash,*, [a] Maciej Kubicki[b]

[a] Department of Inorganic Chemistry, Shahid Beheshti University, 19839 69411 Tehran, Iran.

[b] Faculty of Chemistry, Adam Mickiewicz University, Poznań, Uniwersytetu Poznanskiego 8, 61-614 Poznań, Poland.

E-mail: b_notash@sbu.ac.ir; Tel: +98 2129904363; Fax:+98 2122431663.

List of Supporting Information provided in this file

Synthesis of ligand 4,4-pbubp[1]: Isonicotinic acid hydrazide (6 mmol, 822 mg) was dissolved in 20 ml 25% aq. HCl at 0 °C and $NaNO_2$ (10.0 mmol, 689 mg) dissolved in 5 mL ice cold water was added to it with stirring. Stirring was continued for 1 h, maintaining the temperature below 5 °C. The solution was neutralized by adding solid Na_2CO_3 and extracted with 50 mL toluene. The organic extracts were dried over anhydrous Na_2SO_4 and filtered. Benzene-1,4-diamine (3.0 mmol, 324 mg) was added to the filtrate and refluxed for 6 h. The precipitate was filtered and dried to afford white solid powder **4,4-pbubp** in 70% yield. ^{1}H NMR (DMSO-d_6, 300 MHz): δ= 9.12(s, 1H), 8.83(s, 1H), 8.36-8.37(d, 2H), 7.44-7.45(d, 2H) & 7.41(s, 4H). ^{13}C NMR (DMSO-d_6, 75 MHz) δ= 114.87, 121.97, 136.54, 149.22, 152.71 & 154.80. m.p >260 °C. IR data (KBr pellet, cm^{-1}) (Fig. S3): 3349(w), 3028(w), 1921(w), 1812(w), 1706(s), 1671(s), 1602(s), 1558(m), 1412(m), 1331(m), 1291(m), 1248(m), 1205(m), 1044(m), 990(m), 906(w), 854(m), 820(m), 796(m), 769(m), 748(w), 734(m), 651(s), 575(s), 535(s), 506(m), 419(w).

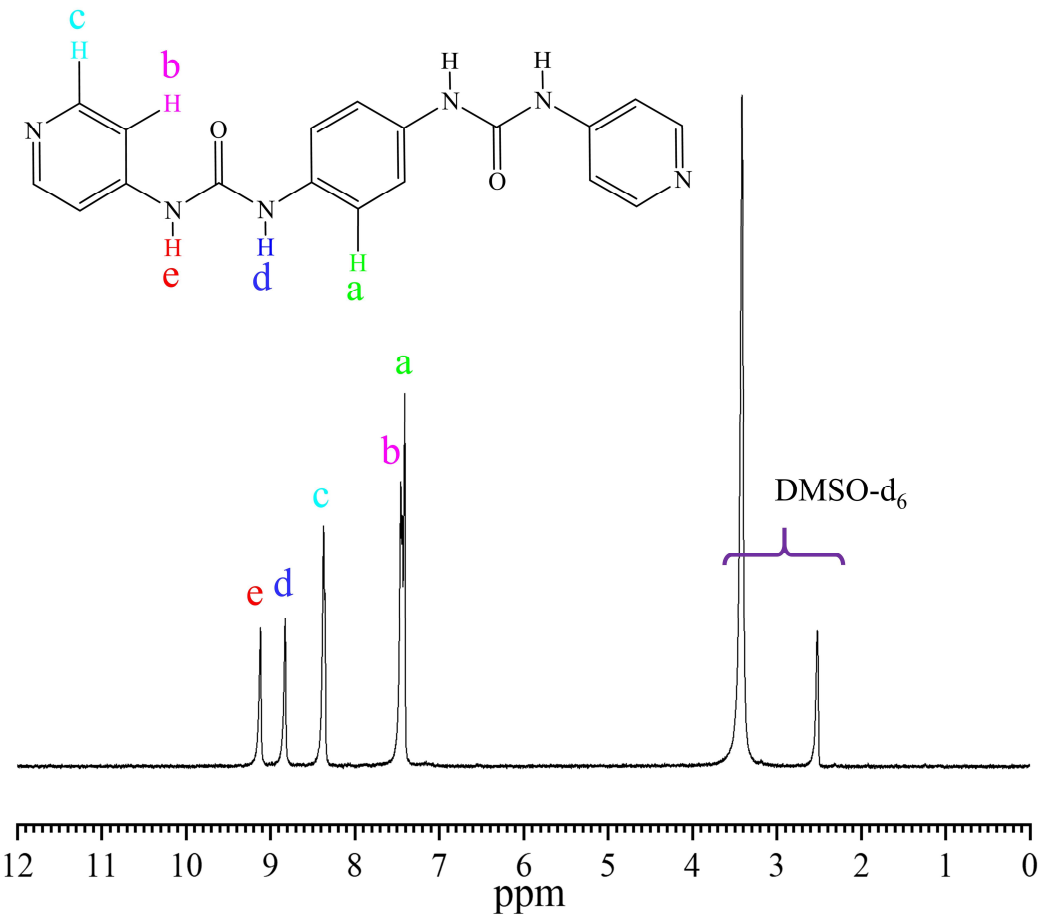

Fig. S1 ^{1}H NMR spectrum of **4,4-pbubp** in DMSO-d_6, 300 MHz.

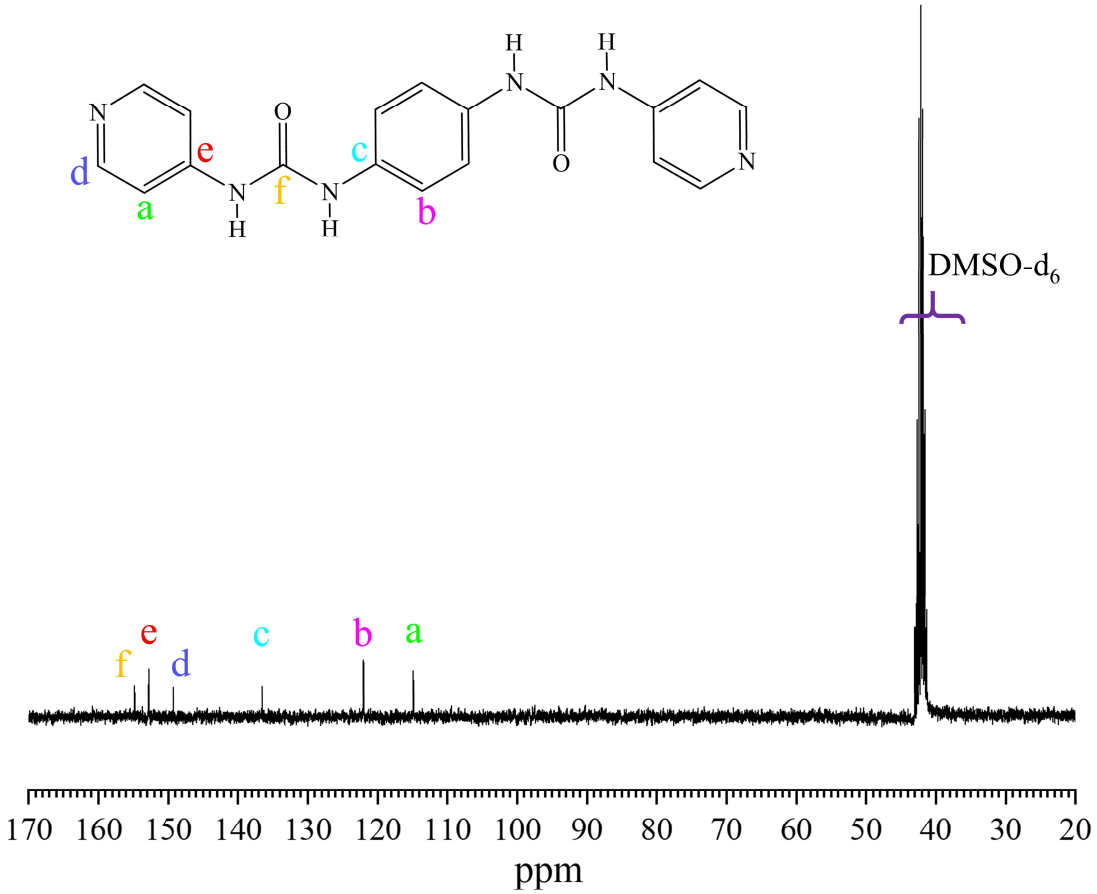

Fig. S2 ^{13}C NMR spectrum of **4,4-pbubp** in DMSO-d_6, 75 MHz.

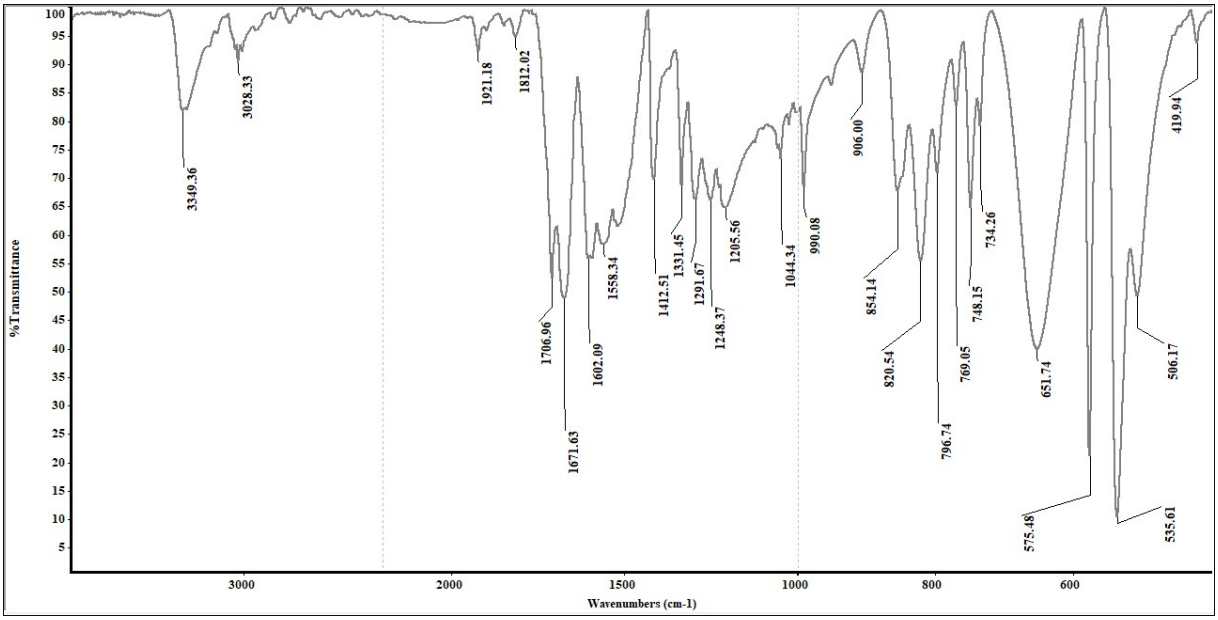

Fig. S3 FT-IR spectrum of ligand **4,4-pbubp** in KBr pellet.

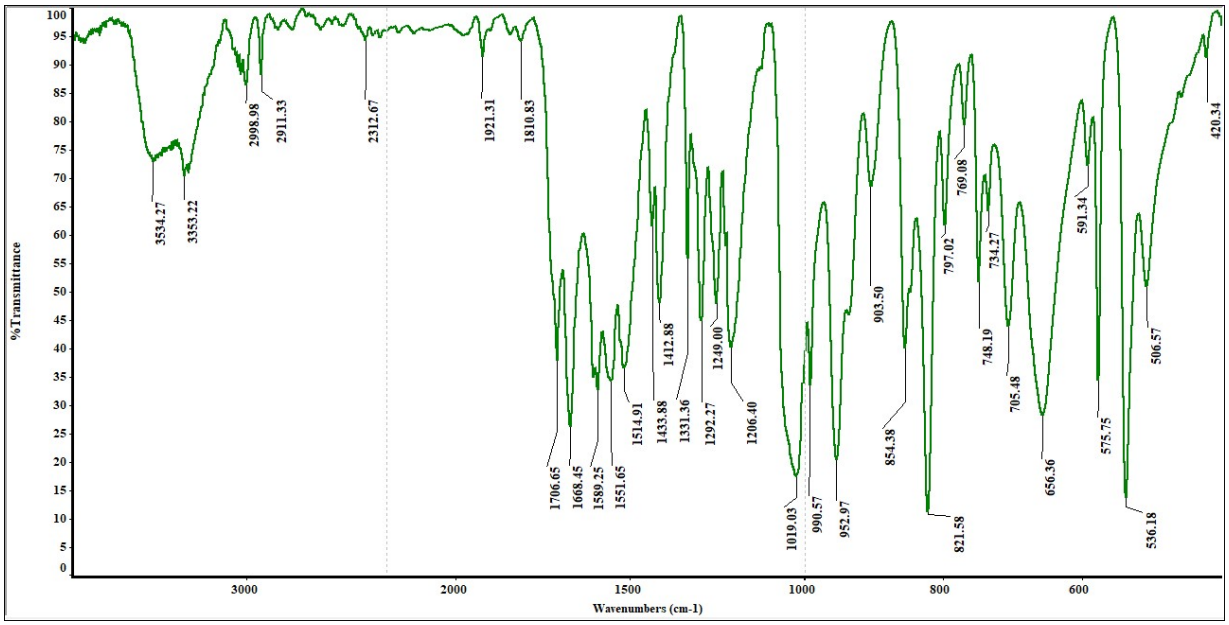

Fig. S4 FT-IR spectrum of **CP1** in KBr pellet.

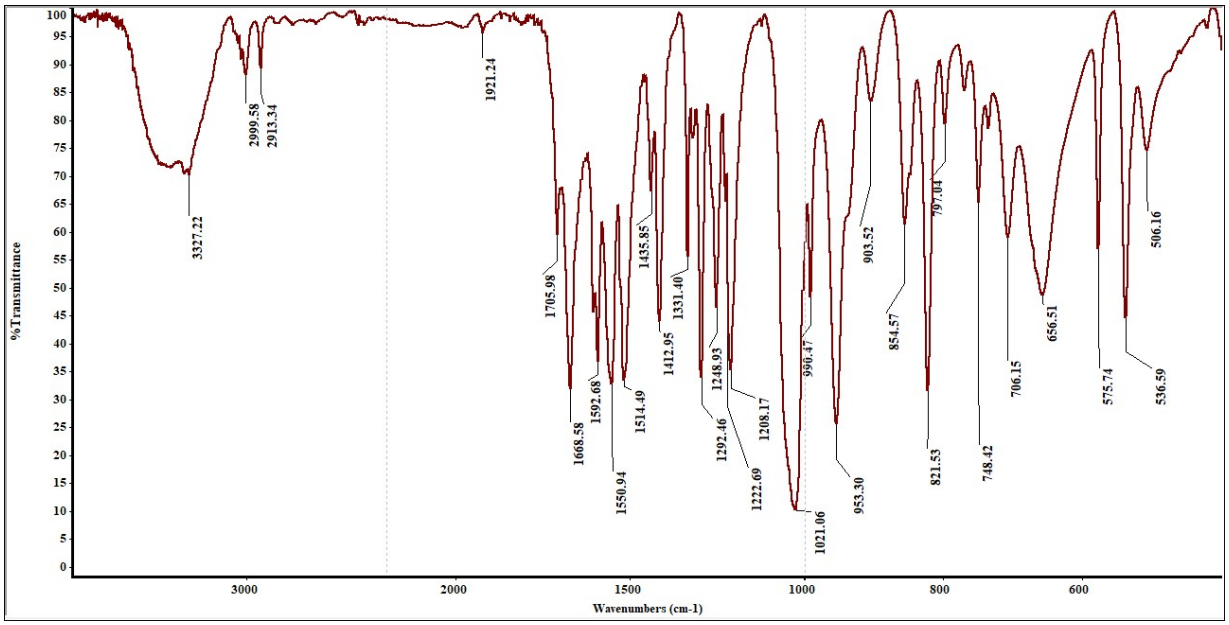

Fig. S5 FT-IR spectrum of **CP2** in KBr pellet.

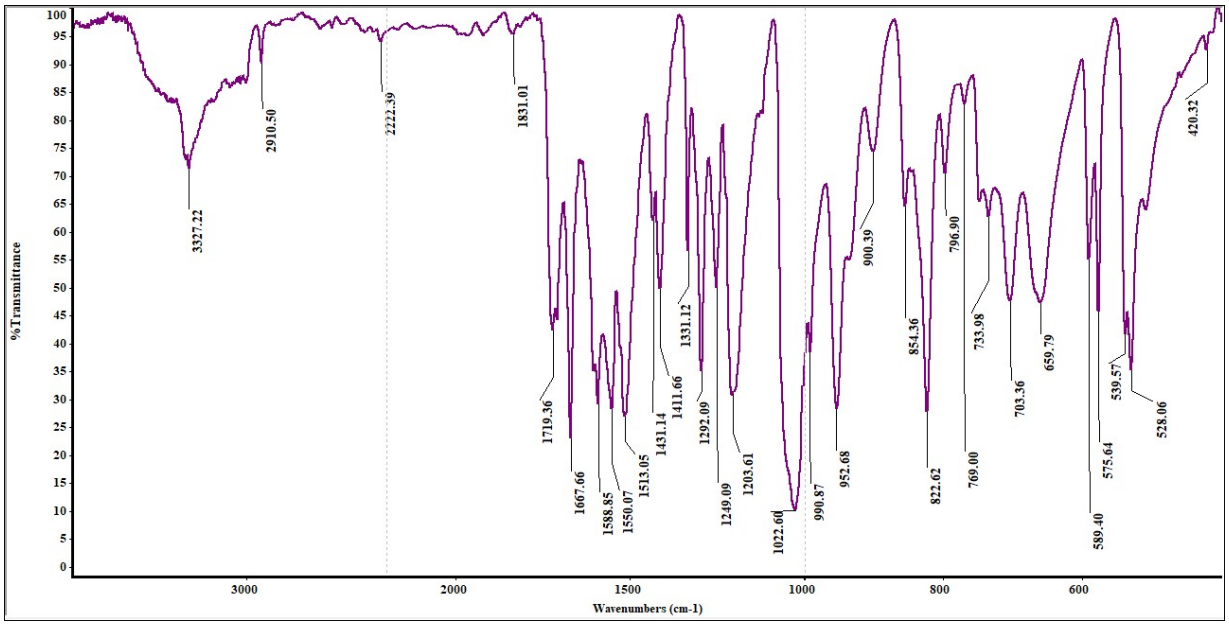

Fig. S6 FT-IR spectrum of **CP3** in KBr pellet.

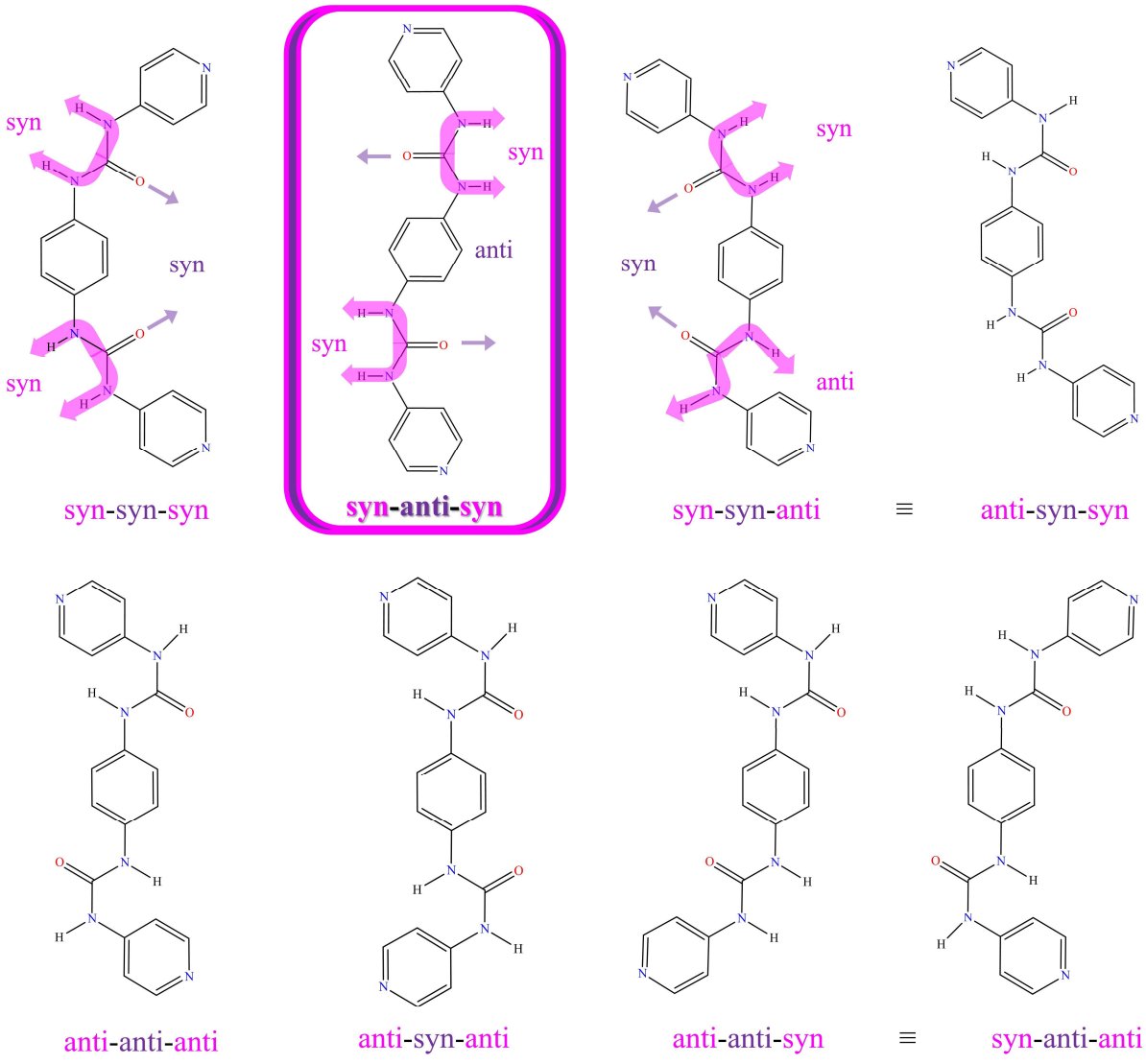

Fig. S7 Plausible conformational isomers for **4,4-pbubp**.

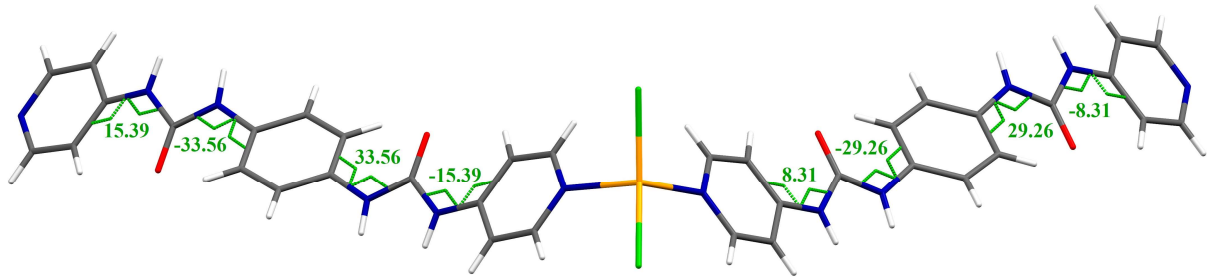

Fig. S8 The dihedral angles between pyridyl rings and urea moieties and between the aromatic rings and the urea moieties of **CP1**.

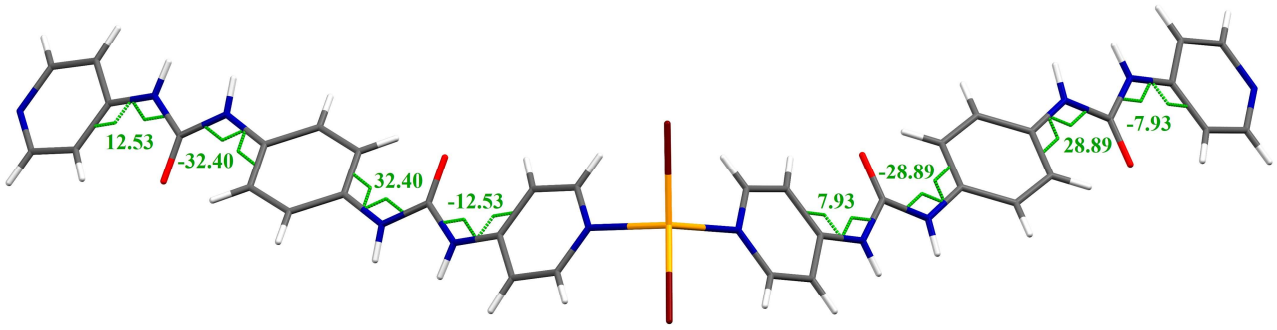

Fig. S9 The dihedral angles between pyridyl rings and urea moieties and between the aromatic rings and the urea moieties of **CP2**.

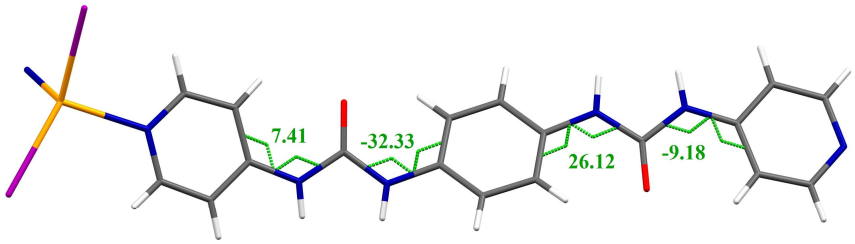

Fig. S10 The dihedral angles between pyridyl rings and urea moieties and between the aromatic rings and the urea moieties of **CP3**.

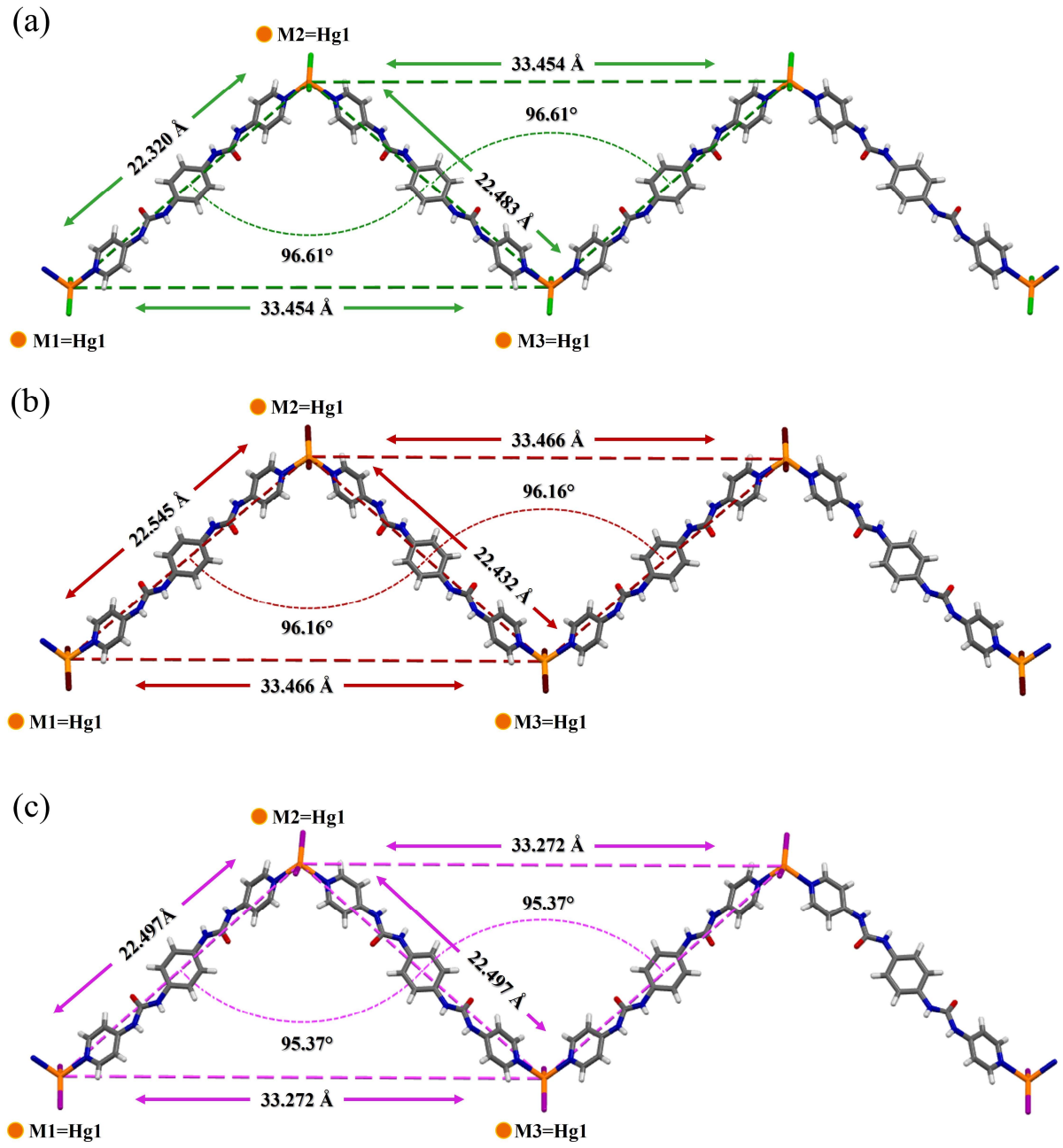

Fig. S11 Hg···Hg distances [Å] and Hg···Hg···Hg angles [^{0}] in zig-zag chains of (a) **CP1**, (b) **CP2** and (c) **CP3**.

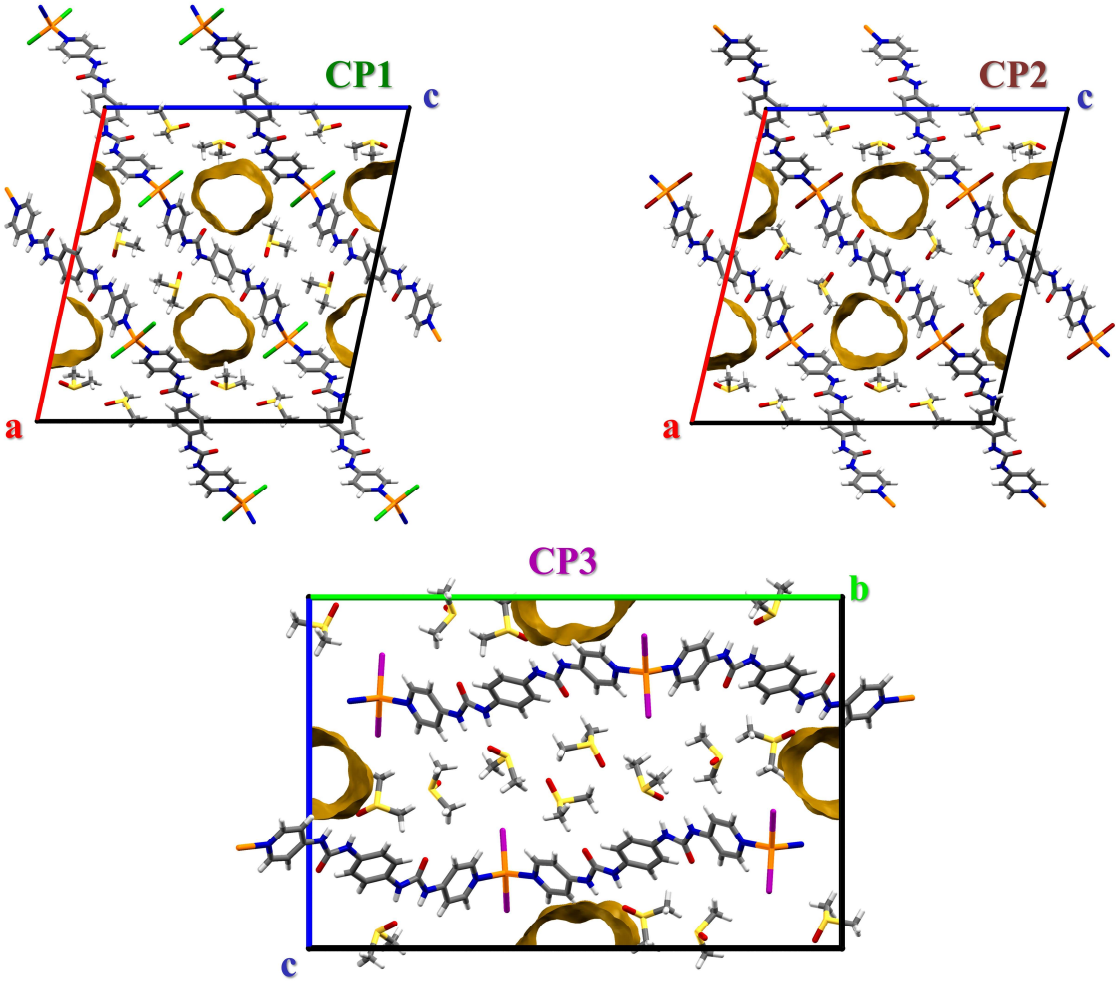

Fig. S12 View of the channels (location of disordered DMSO solvent molecules) in **CP1** and **CP2** along *b*-axis and in **CP3** along *a*-axis.

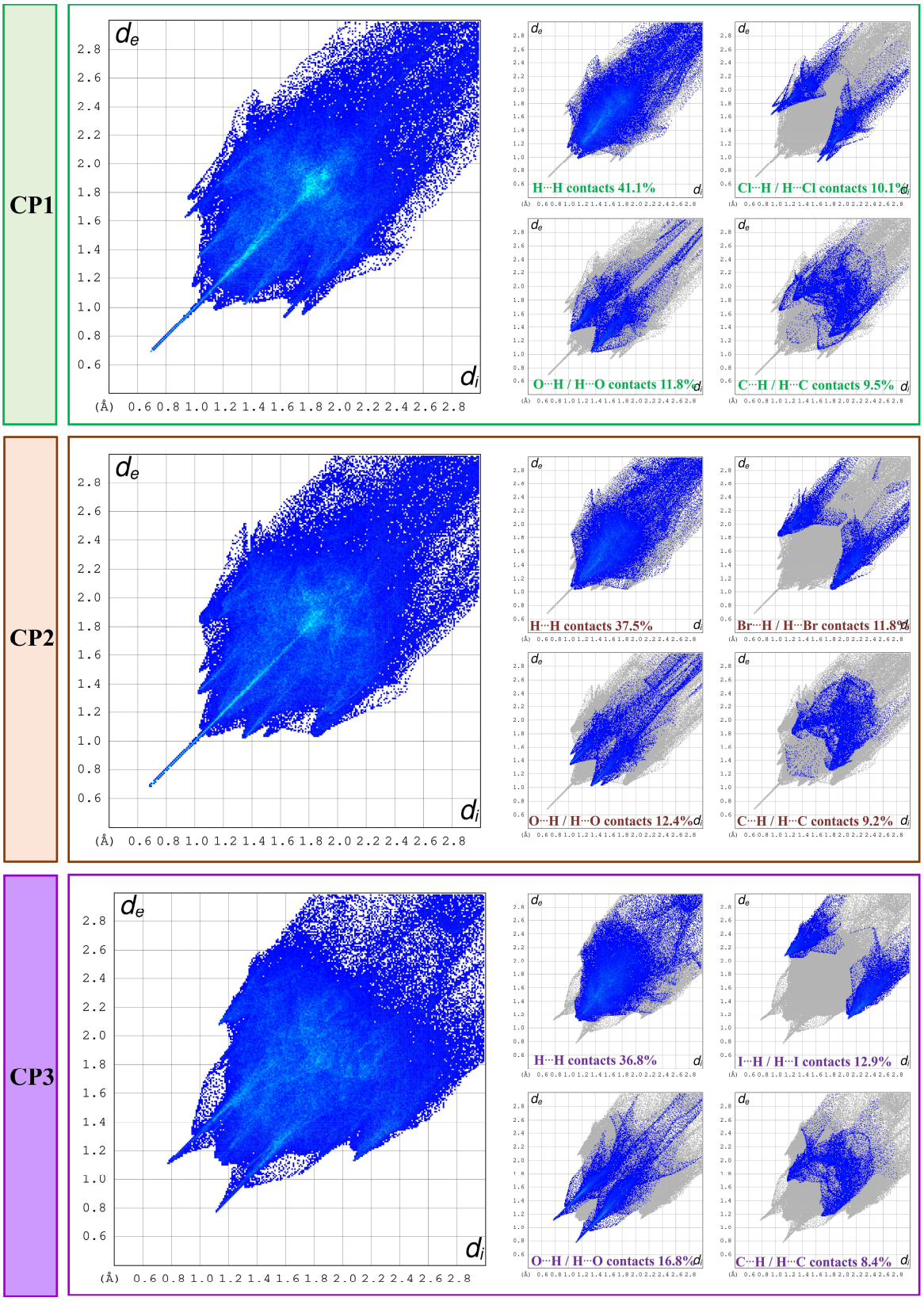

Fig. S13 2D fingerprint plots for **CP1**, **CP2** and **CP3**: Full (left) and resolved into H···H, O···H/H···O, X···H/H···X and C···H/H···C contacts. These plots illustrate the percentages of various contacts contributing to the overall Hirshfeld surface area of the molecules.

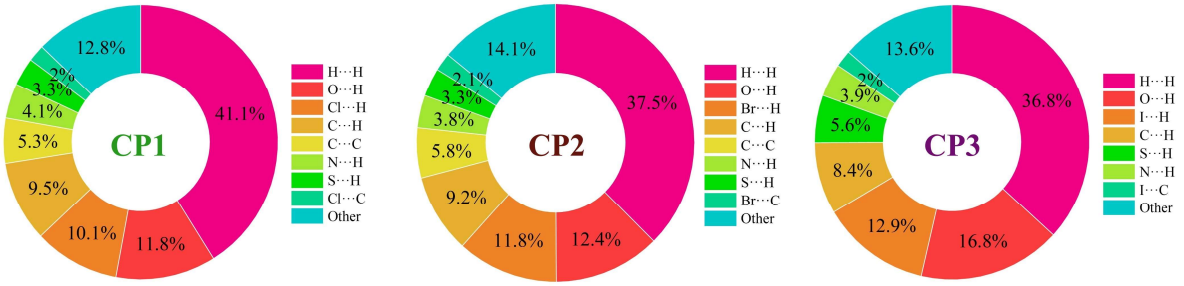

Fig. S14 Distribution of the intermolecular contacts base on Hirshfeld surface analysis for **CP1**, **CP2** and **CP3**.

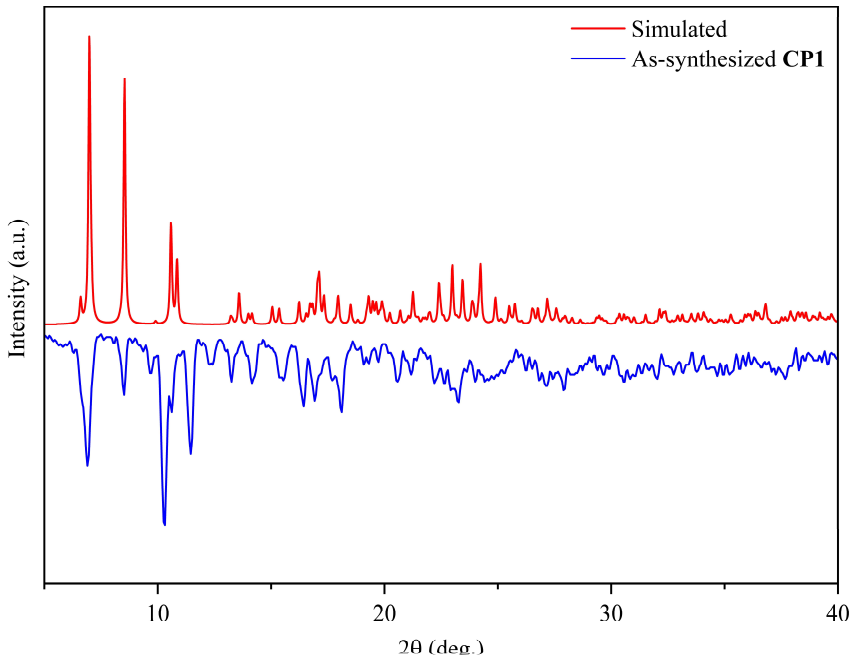

Fig. S15 PXRD patterns of **CP1**. Red: Simulated from the X-ray single crystal data; Blue: observed for the as-synthesized solids.

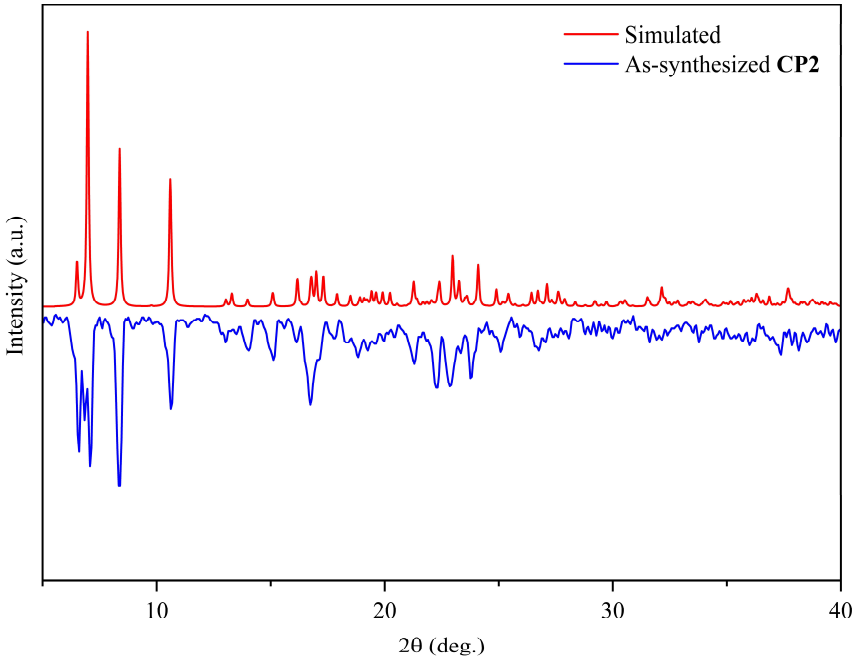

Fig. S16 PXRD patterns of **CP2**. Red: Simulated from the X-ray single crystal data; Blue: observed for the as-synthesized solids.

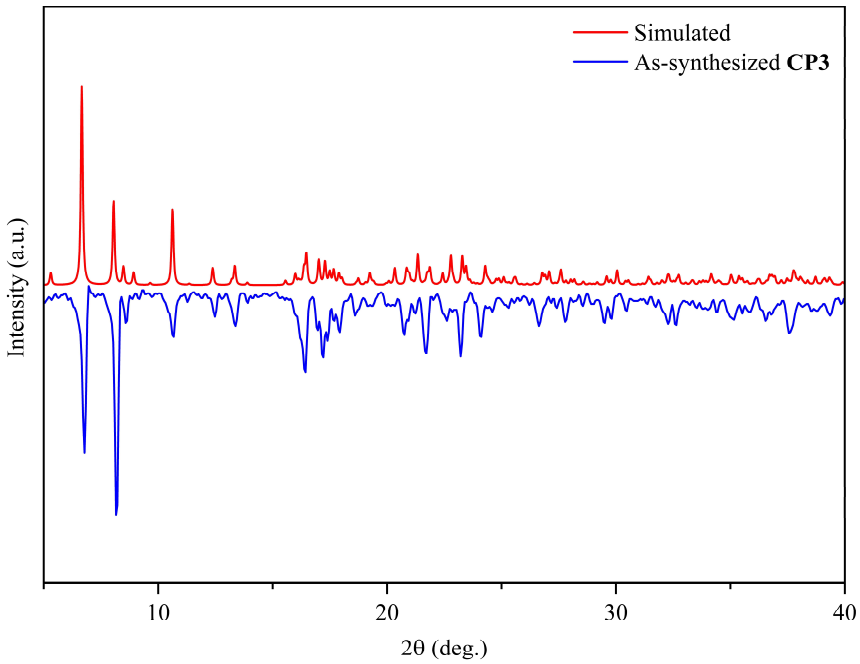

Fig. S17 PXRD patterns of **CP3**. Red: Simulated from the X-ray single crystal data; Blue: observed for the as-synthesized solids.

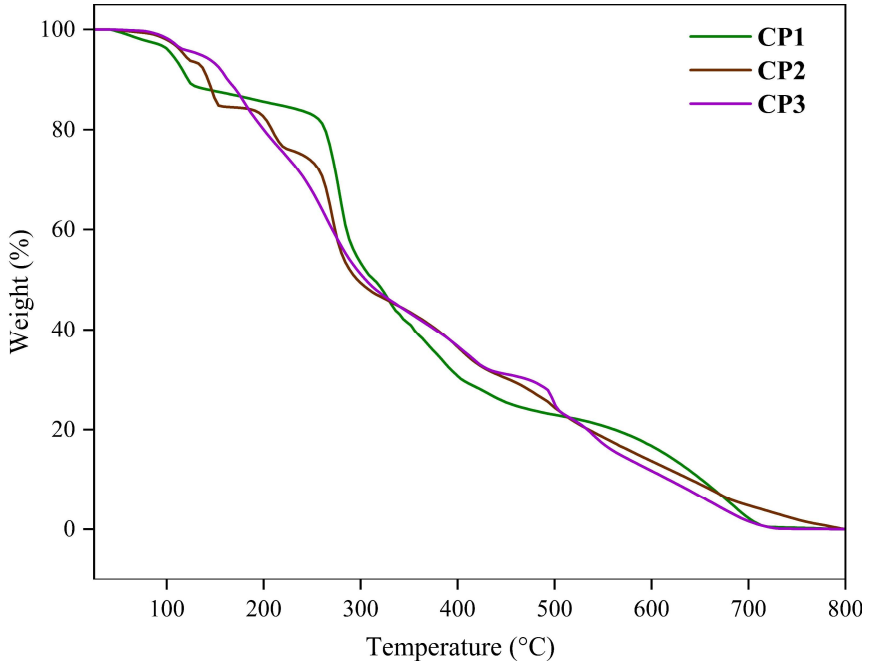

Fig. S18 TGA curves of **CP1**, **CP2** and **CP3**.

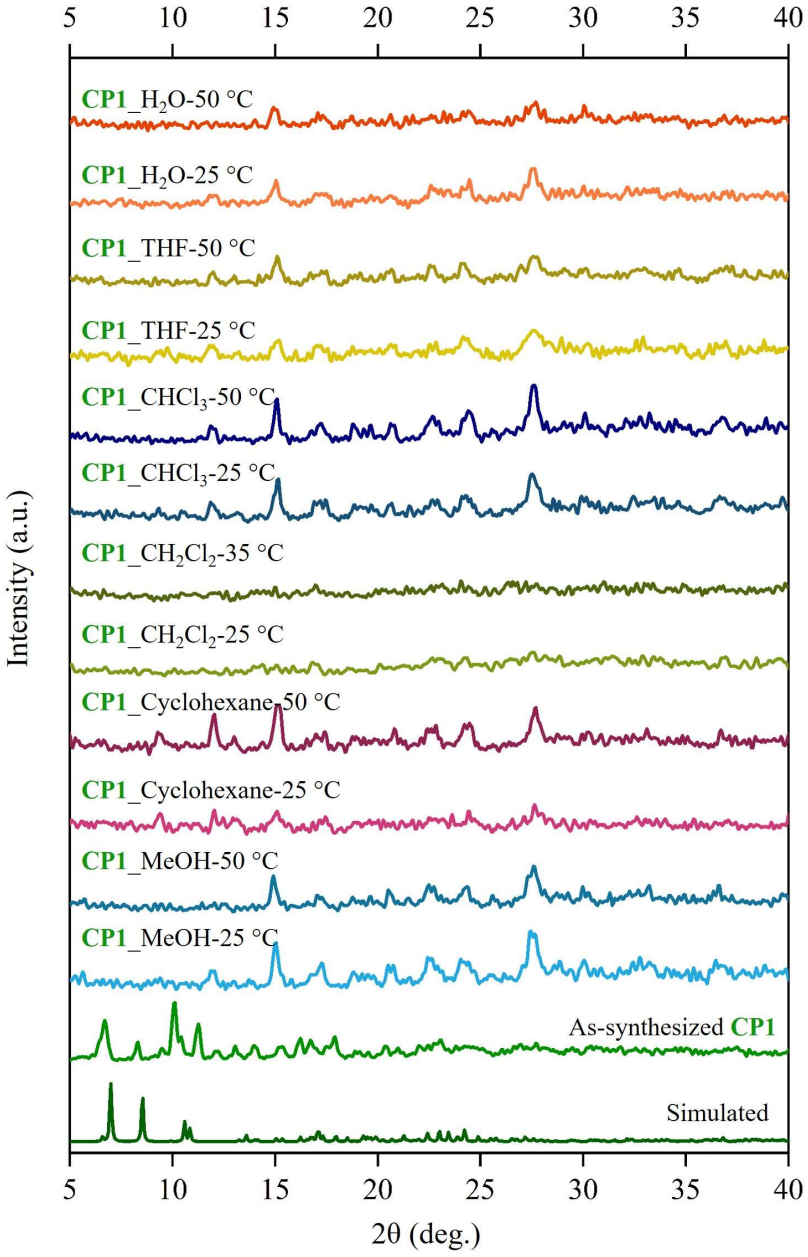

Fig. S19 PXRD patterns of **CP1**: simulated, as-synthesized, and after immersion in H_2O and different organic solvents for 1 h, at 25 and 50 °C.

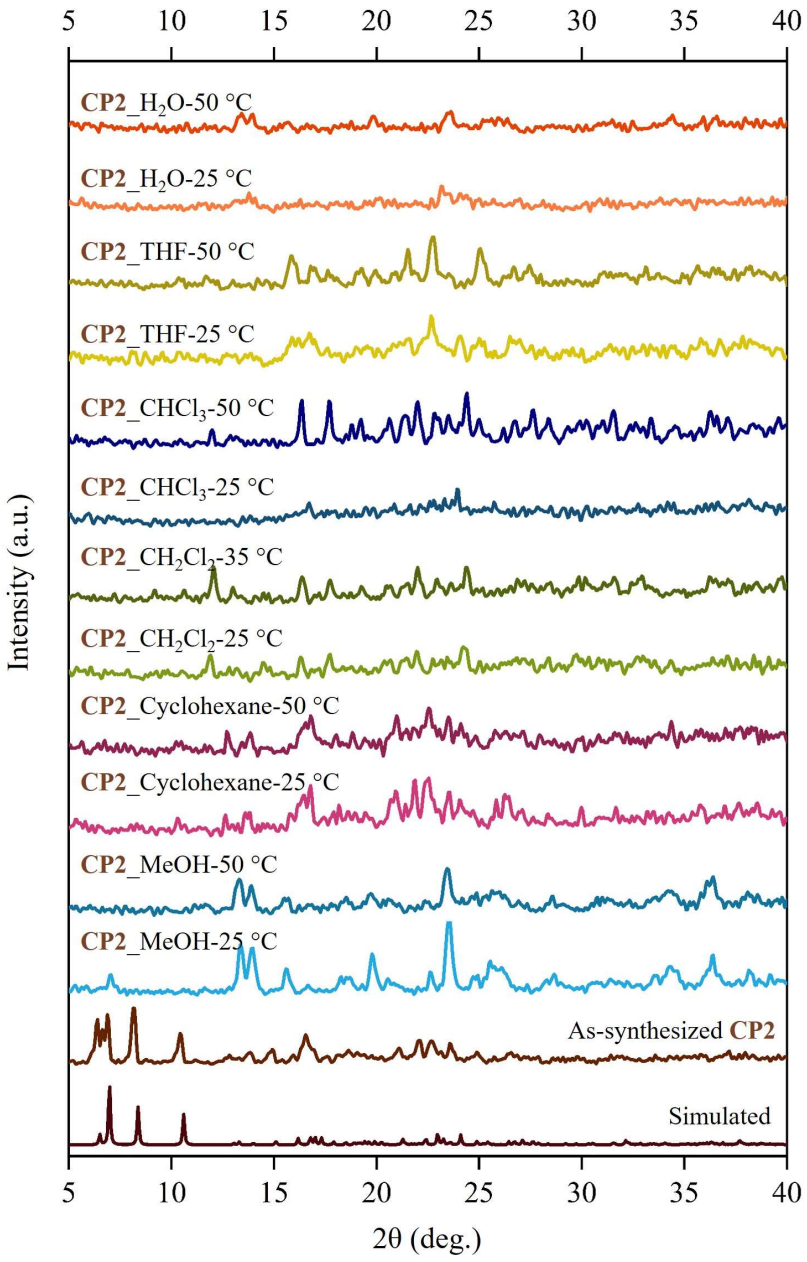

Fig. S20 PXRD patterns of **CP2**: simulated, as-synthesized, and after immersion in H_2O and different organic solvents for 1 h, at 25 and 50 °C.

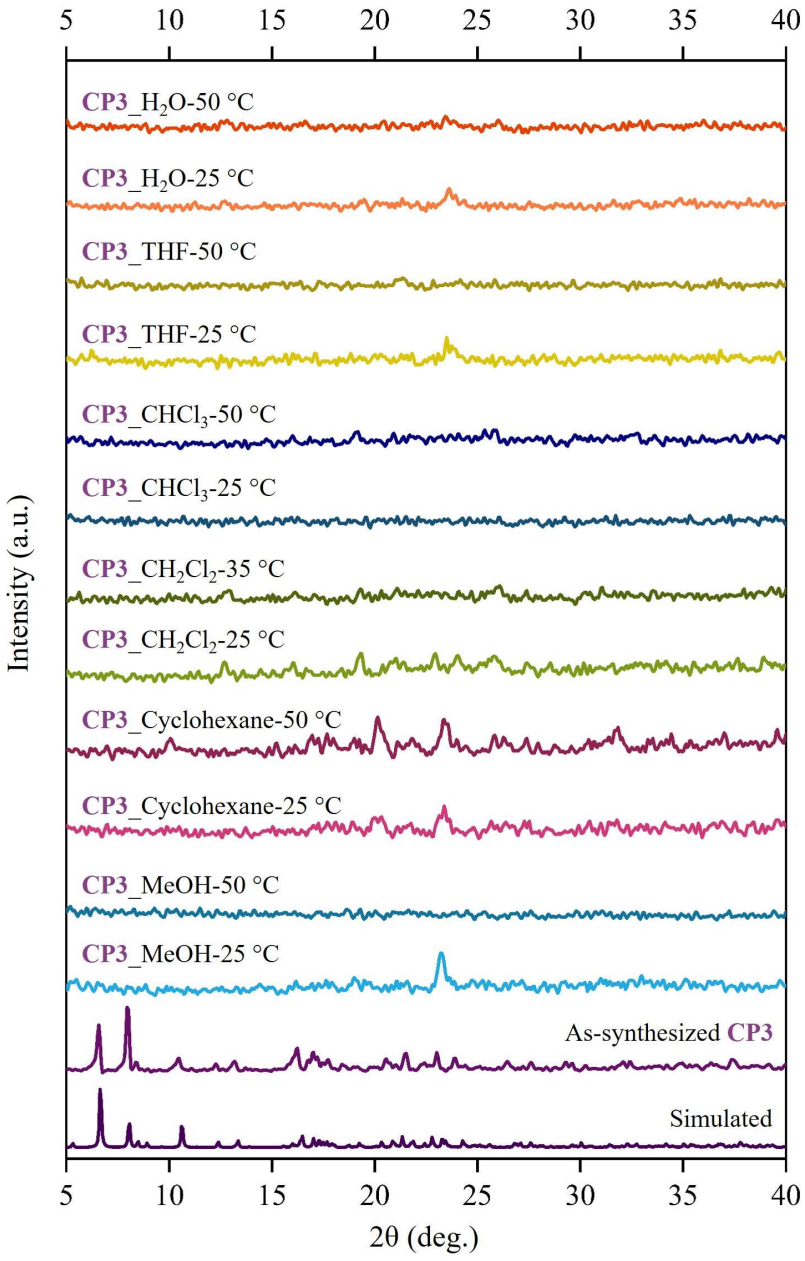

Fig S21 PXRD patterns of **CP3**: simulated, as-synthesized, and after immersion in H_2O and different organic solvents for 1 h, at 25 and 50 °C.

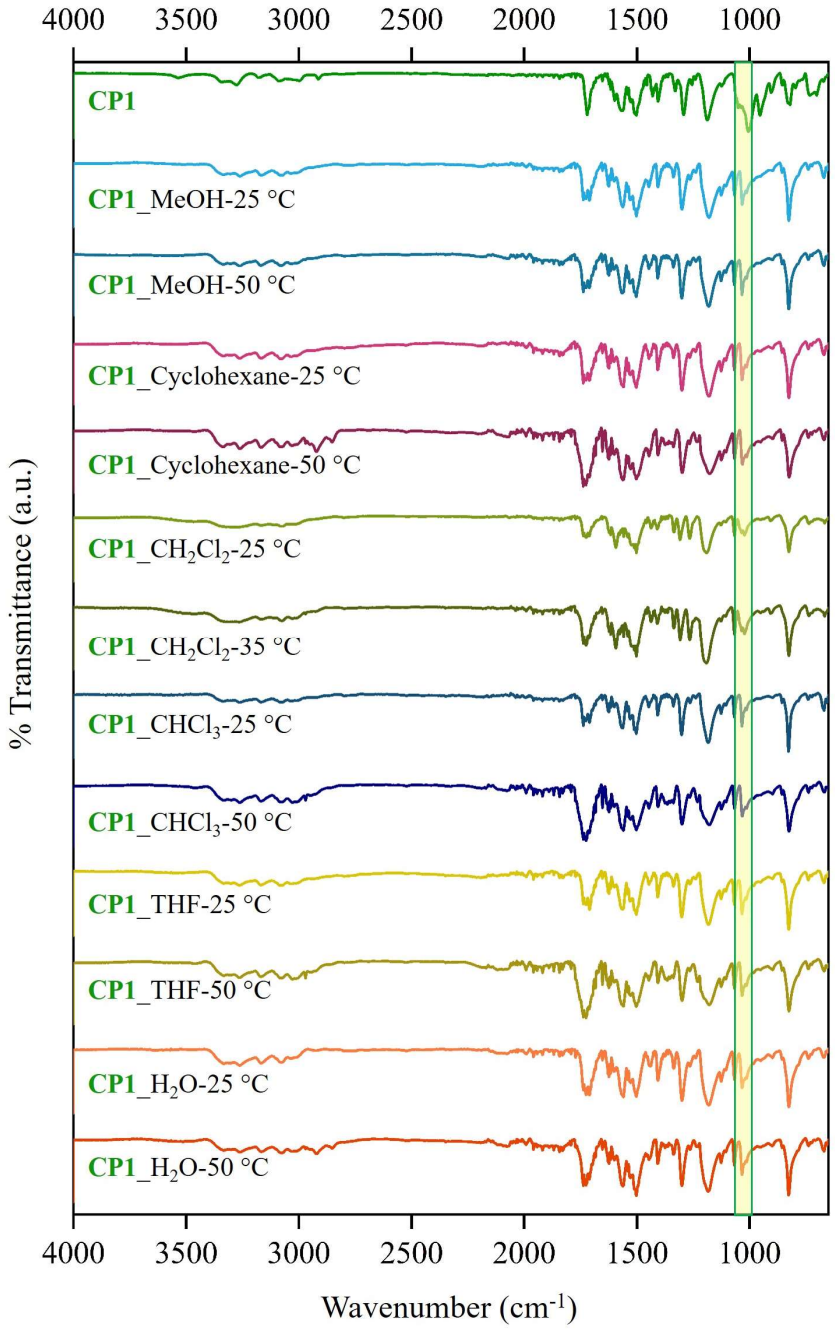

Fig S22 ATR-FTIR spectra of **CP1**: as-synthesized, and after immersion in H_2O and different organic solvents for 1 h, at 25 and 50 °C.

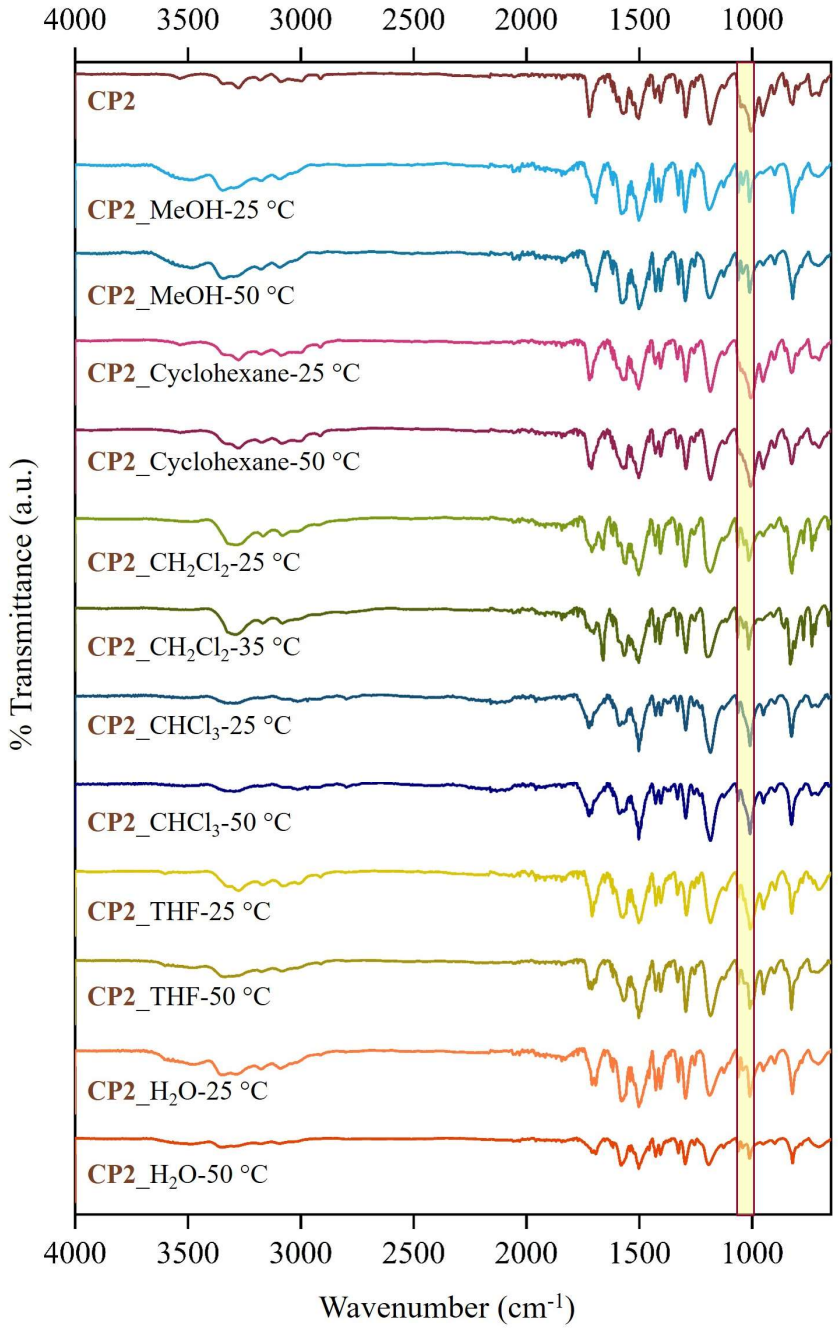

Fig S23 ATR-FTIR spectra of **CP2**: as-synthesized, and after immersion in H_2O and different organic solvents for 1 h, at 25 and 50 °C.

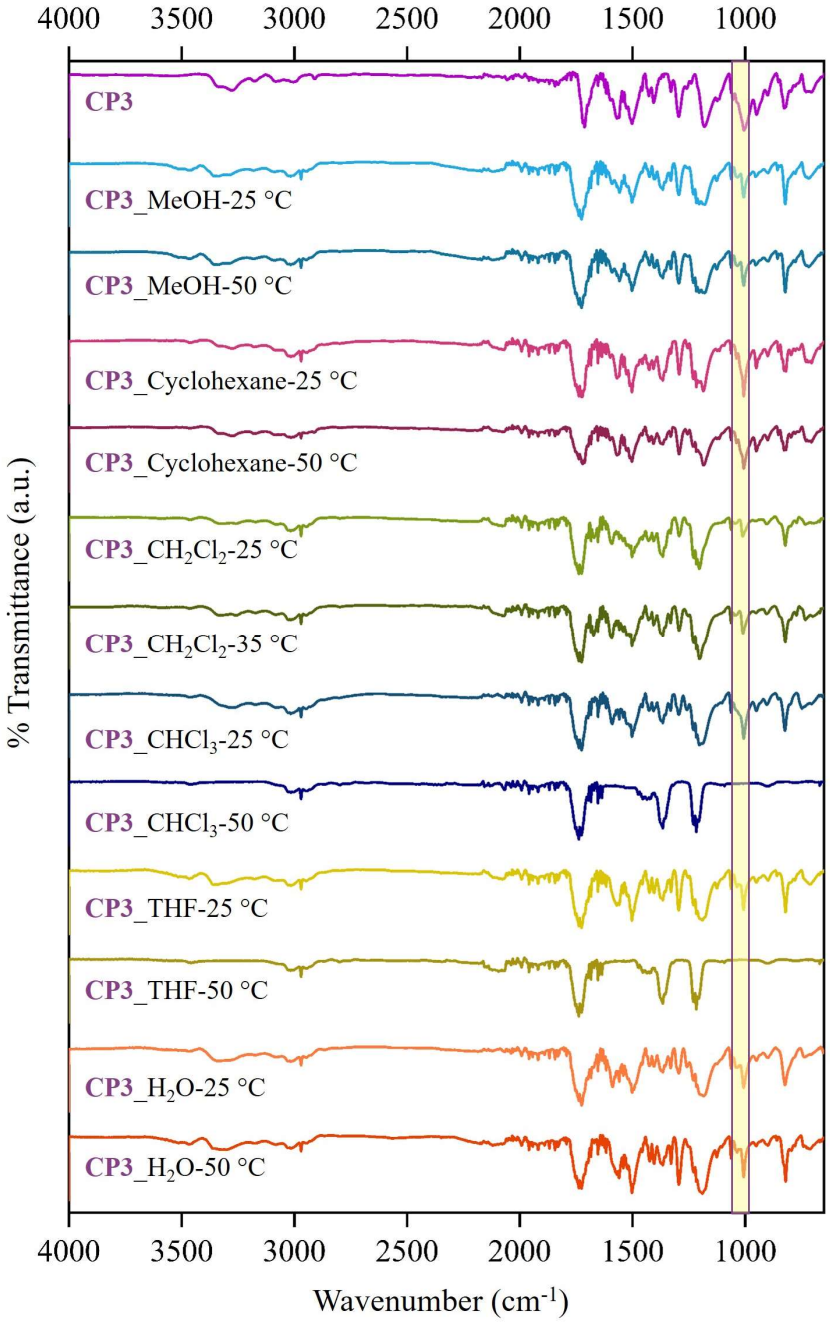

Fig S24 ATR-FTIR spectra of **CP3**: as-synthesized, and after immersion in H_2O and different organic solvents for 1 h, at 25 and 50 °C.

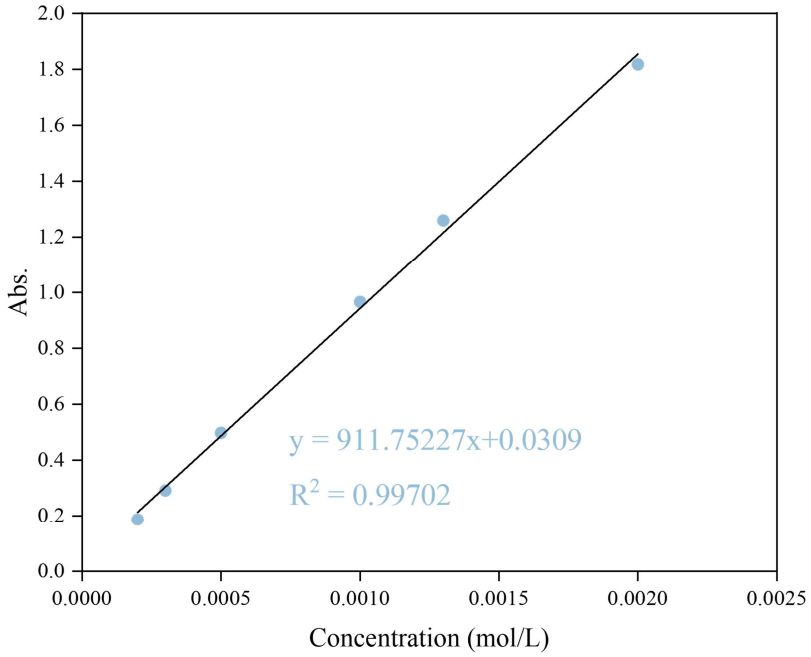

Fig. S25 Calibration plot of standard iodine in cyclohexane by UV-Vis spectra.

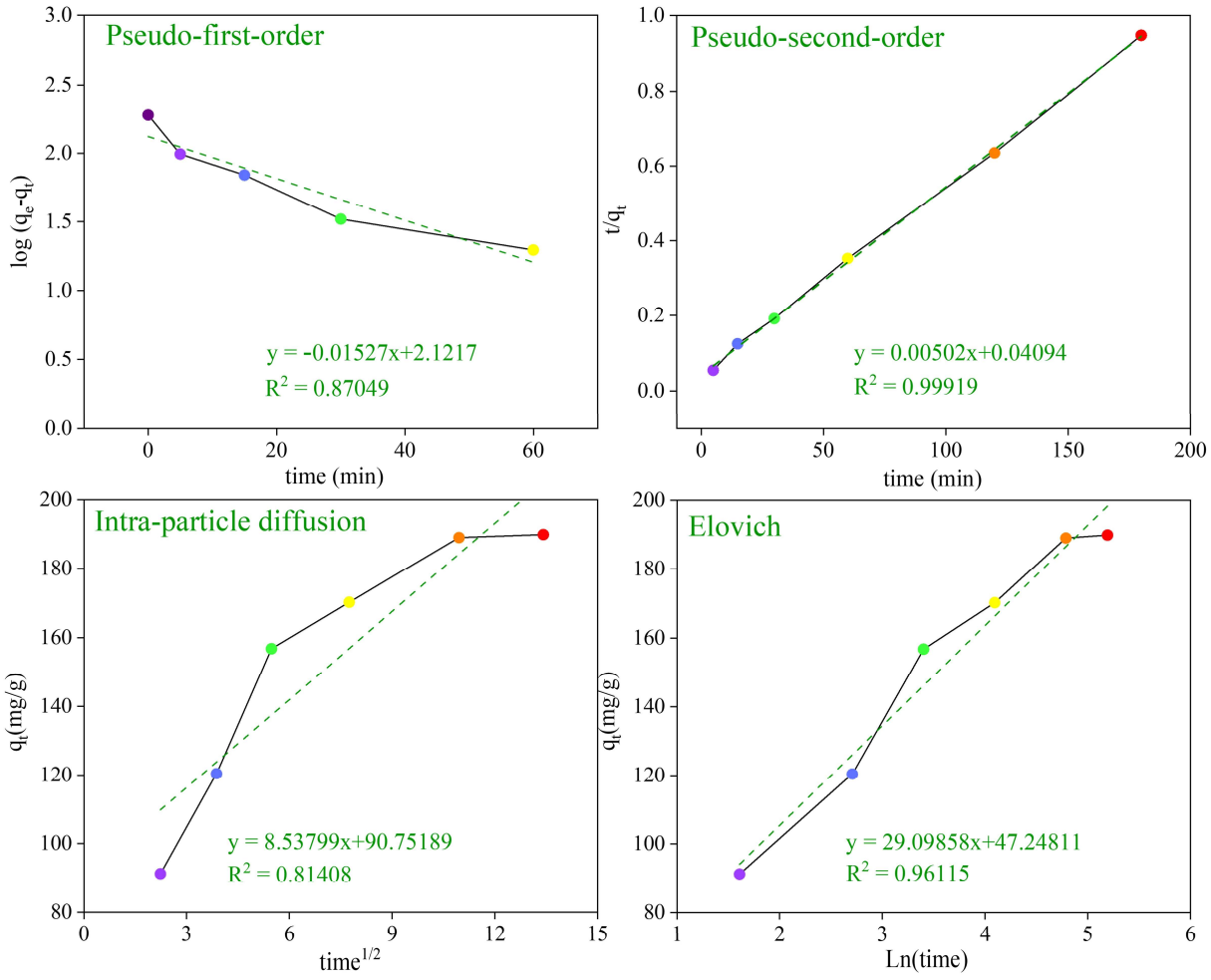

Fig. S26 The pseudo-first-order, pseudo-second-order, intraparticle diffusion, and Elovich models for the uptake of I_2 by compound **CP1** at 0.005 M concentration of solution.

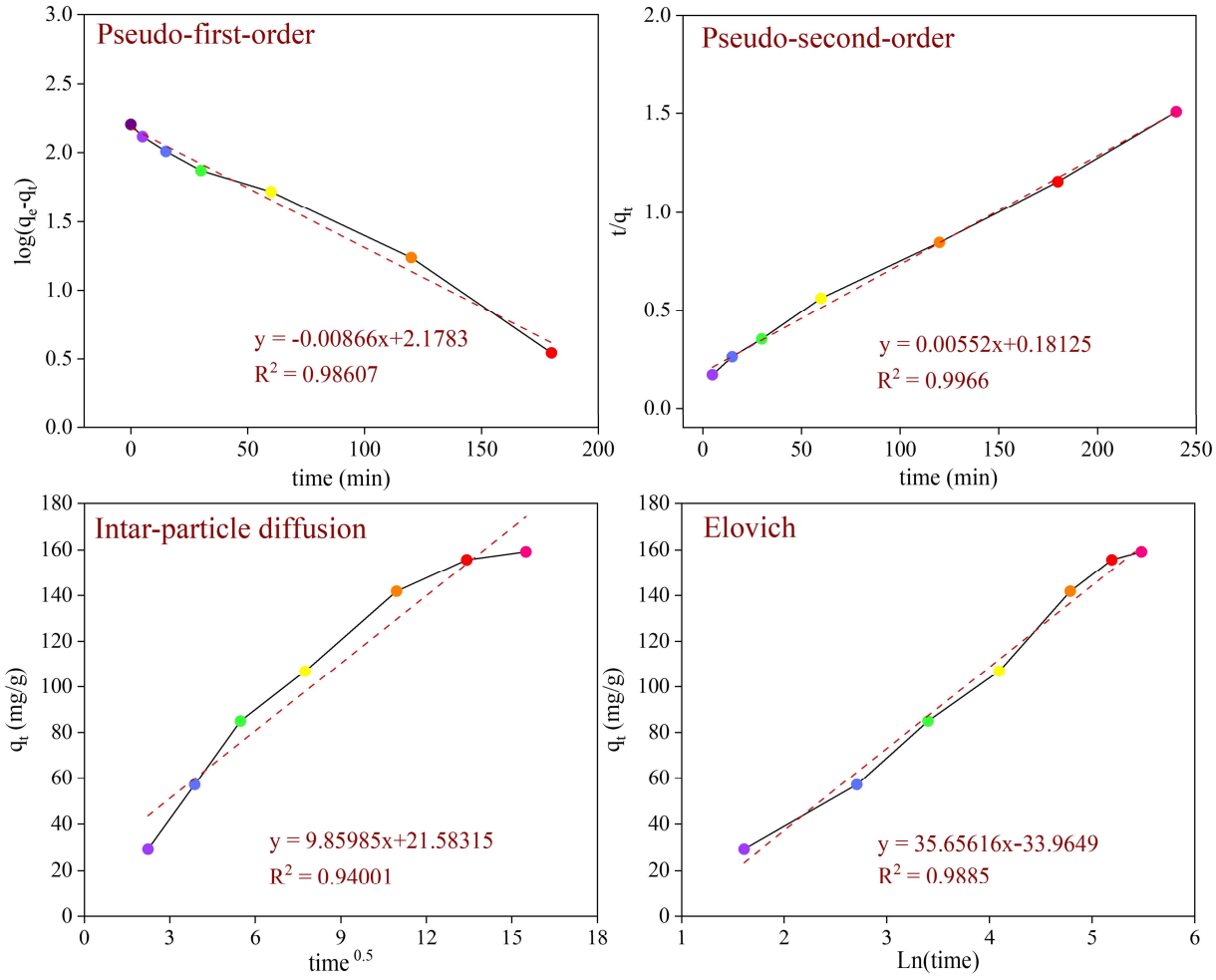

Fig. S27 The pseudo-first-order, pseudo-second-order, intraparticle diffusion, and Elovich models for the uptake of I_2 by compound **CP2** at 0.005 M concentration of solution.

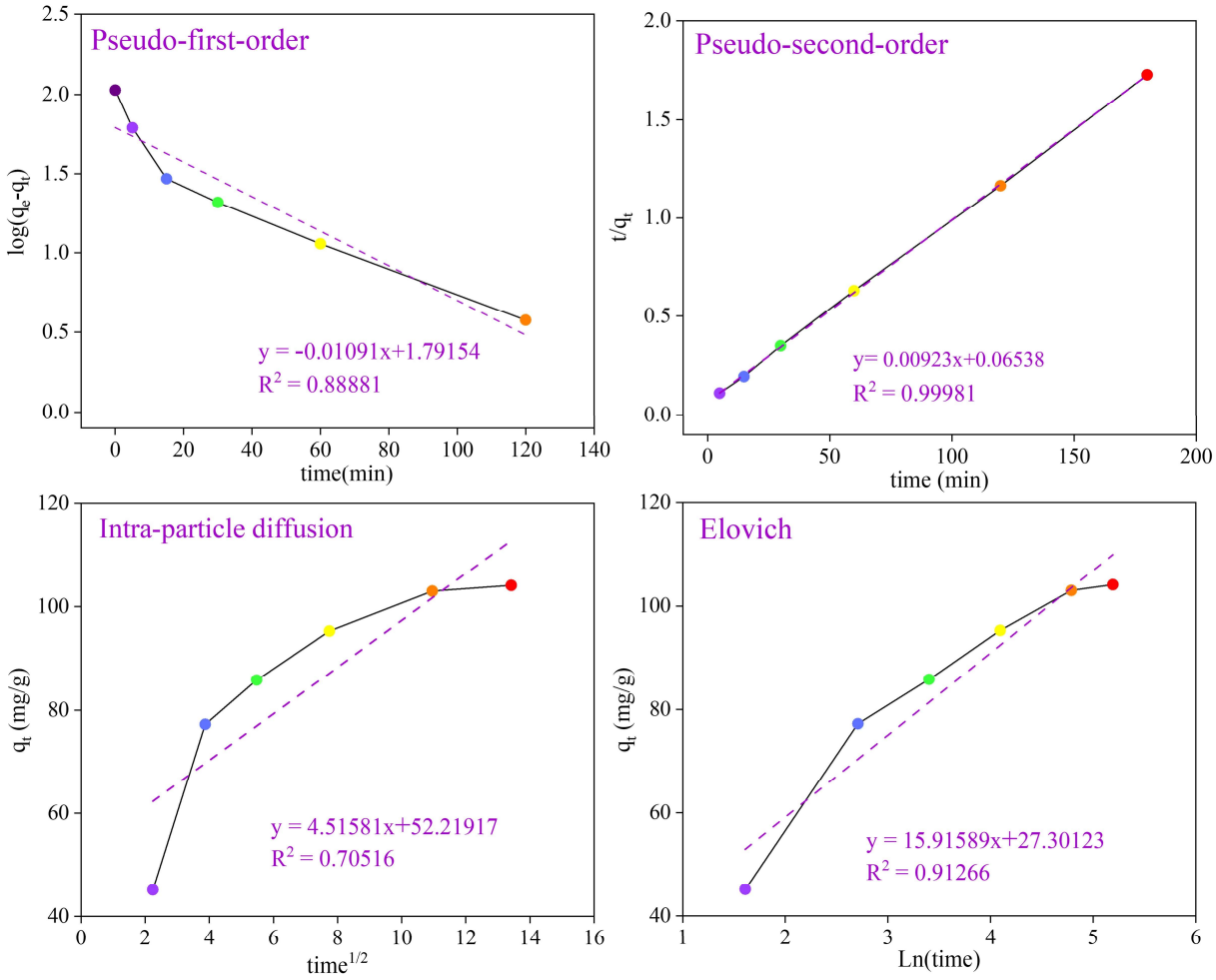

Fig. S28 The pseudo-first-order, pseudo-second-order, intraparticle diffusion, and Elovich models for the uptake of I_2 by compound **CP3** at 0.005 M concentration of solution.

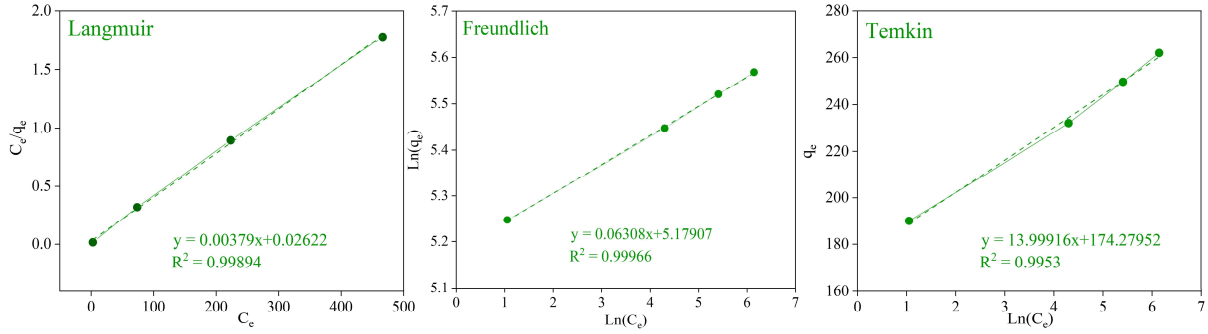

Fig. S29 The Langmuir, Temkin, and Freundlich isotherm models for compound **CP1**.

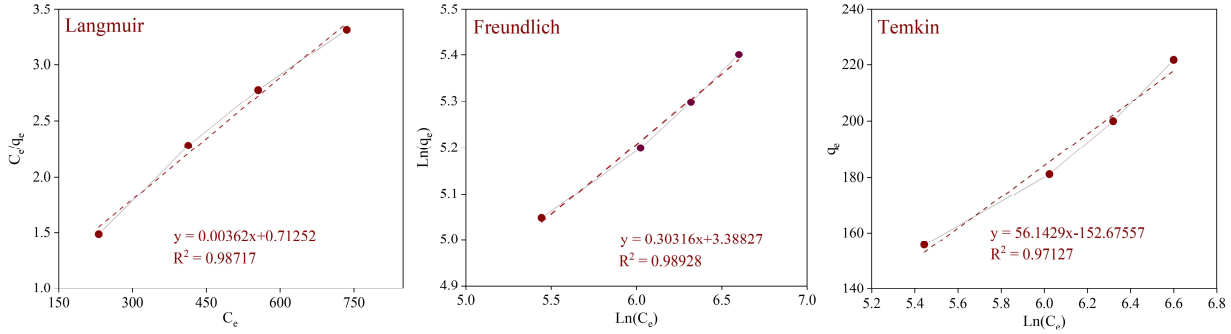

Fig. S30 The Langmuir, Temkin, and Freundlich isotherm models for compound **CP2**.

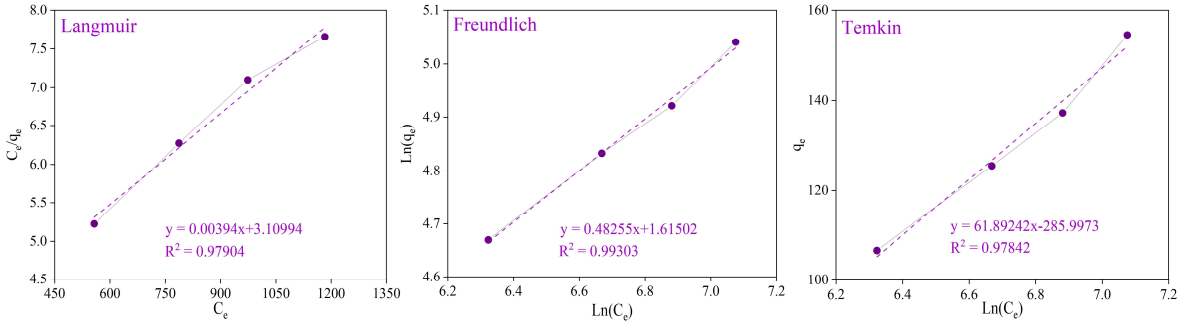

Fig. S31 The Langmuir, Temkin, and Freundlich isotherm models for compound **CP3**.

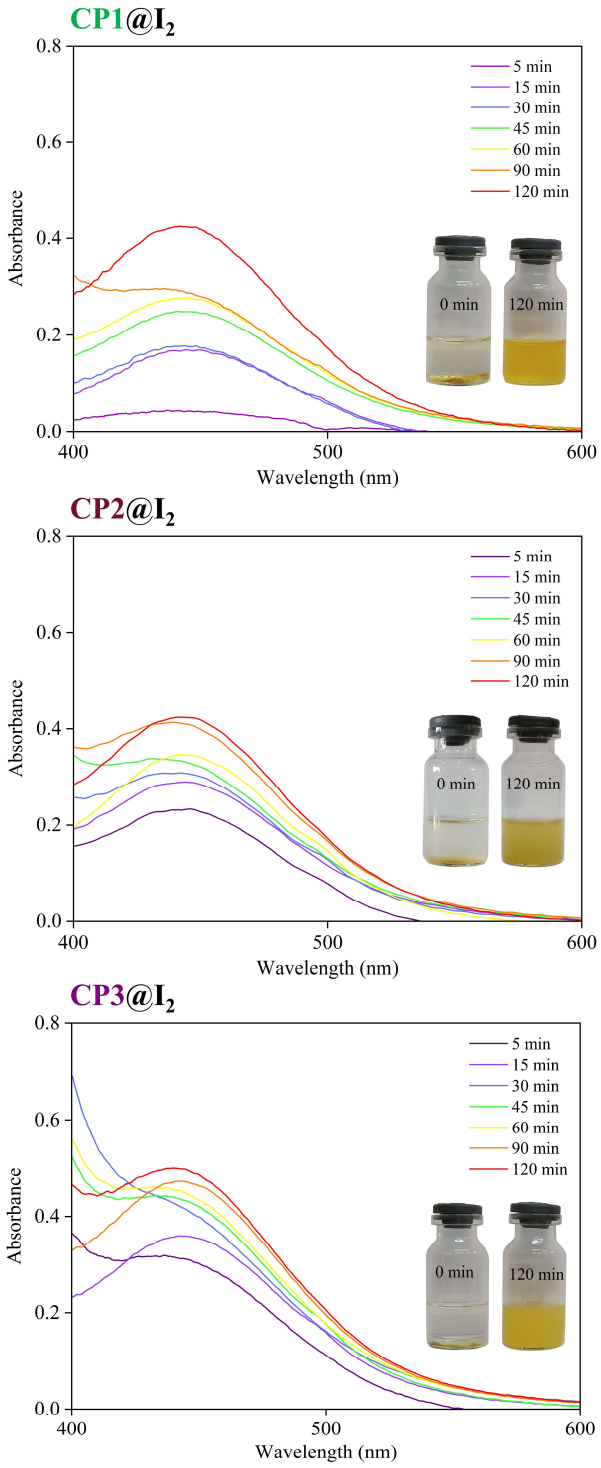

Fig. S32 The UV-Vis spectra of compounds **CP1@I2**, **CP2@I2** and **CP3@I2** immersed in 5 mL ethanol and the photograph of the releasing process at the beginning and after 120 min.

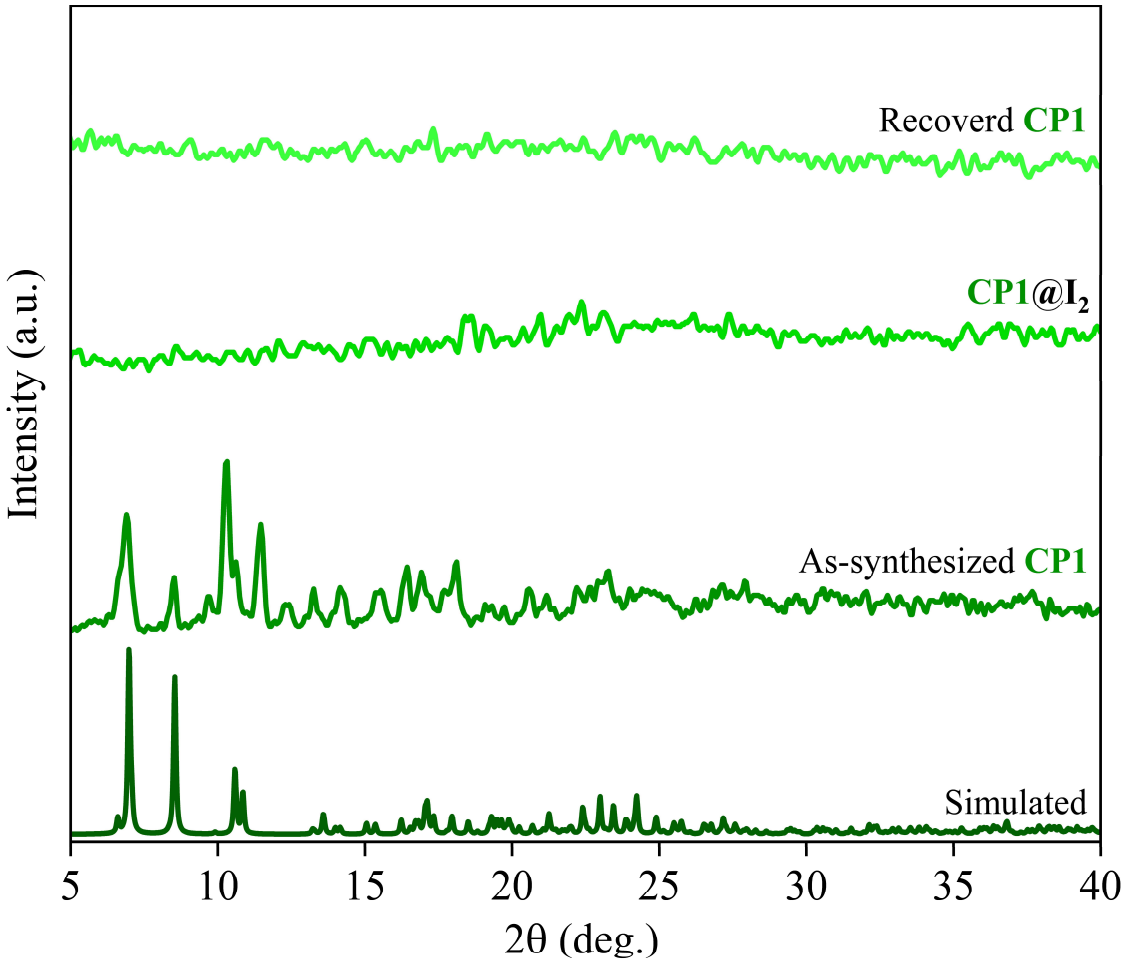

Fig. S33 Comparison between the simulation powder X-ray diffraction patterns of the **CP1**, before iodine uptake, the **CP1@I2** and recovered **CP1**.

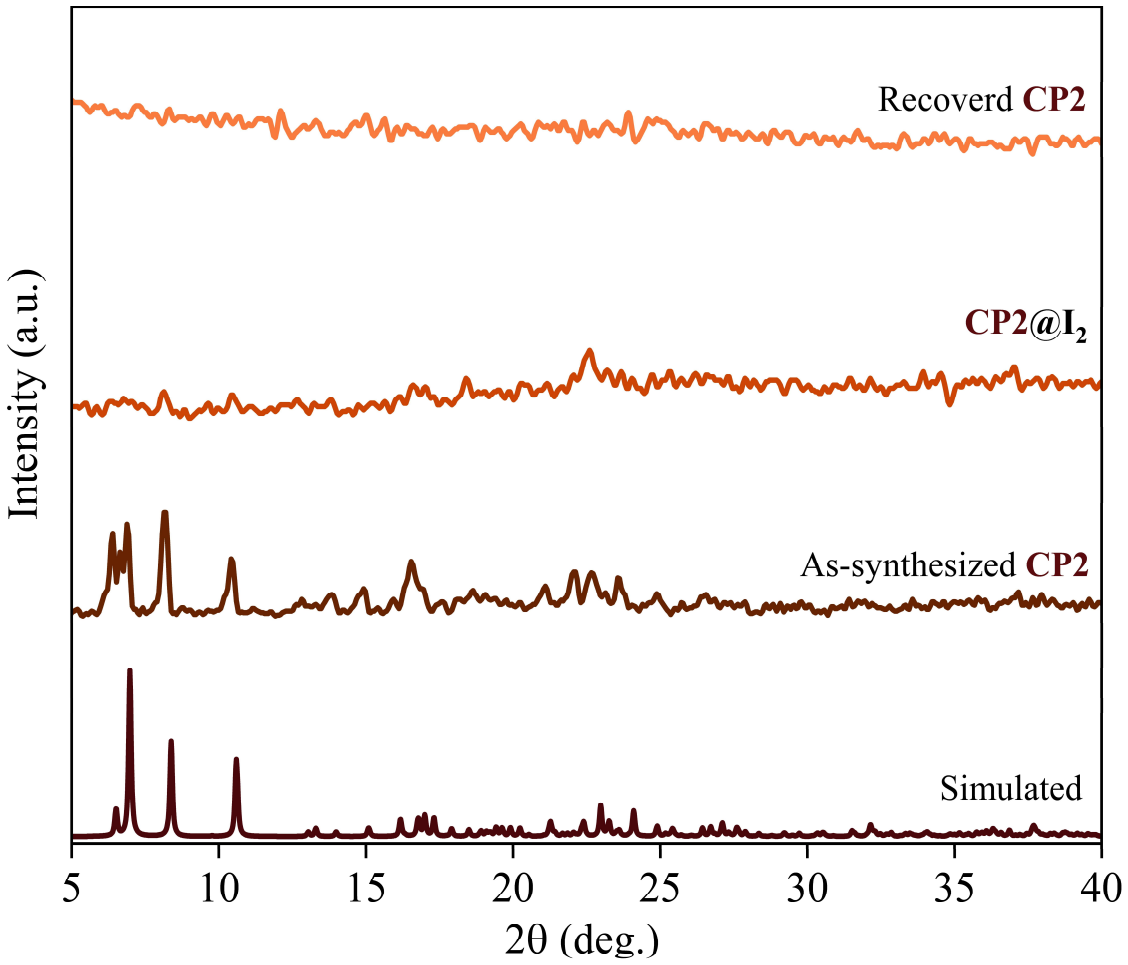

Fig. S34 Comparison between the simulation powder X-ray diffraction patterns of the **CP2**, before iodine uptake, the **CP2@I_2** and recovered **CP2**.

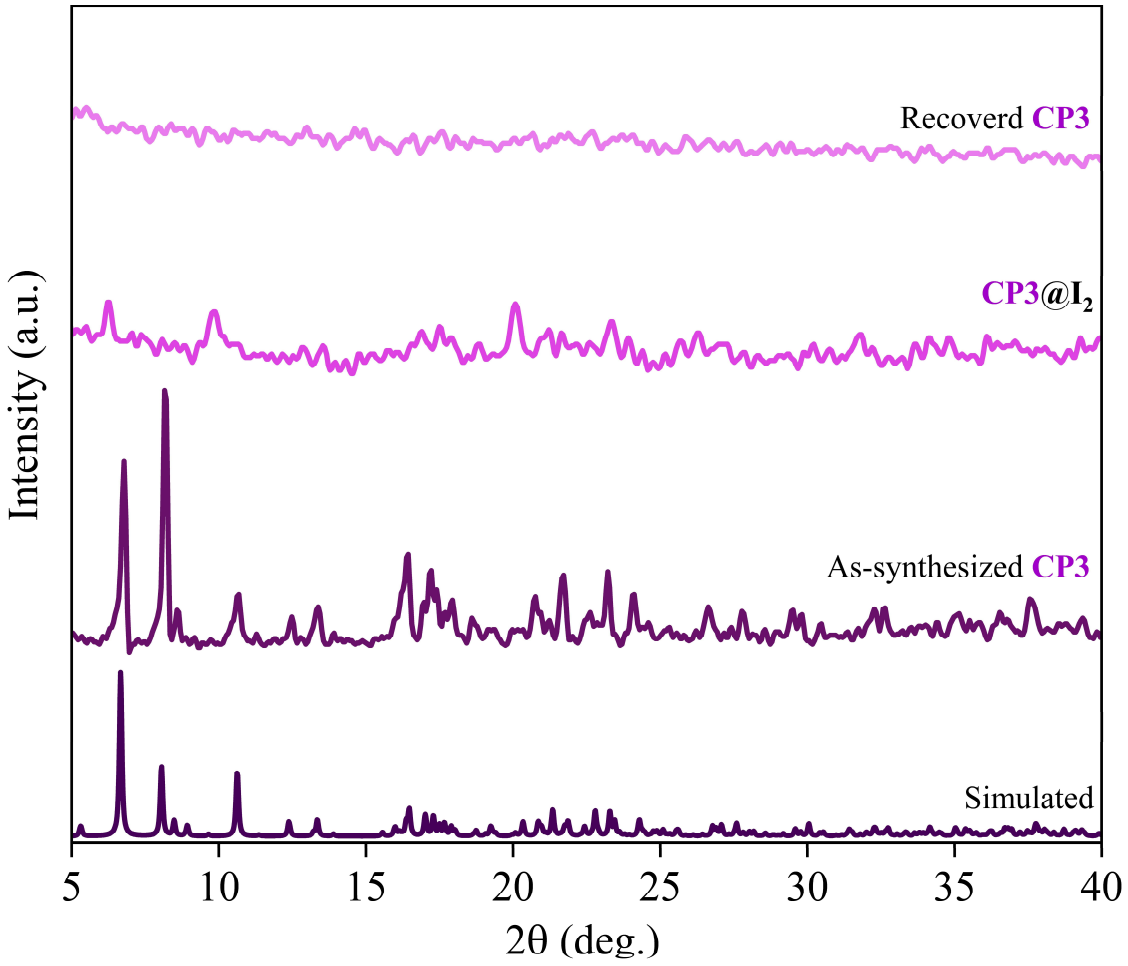

Fig. S35 Comparison between the simulation powder X-ray diffraction patterns of the **CP3**, before iodine uptake, the **CP3@I_2** and recovered **CP3**.

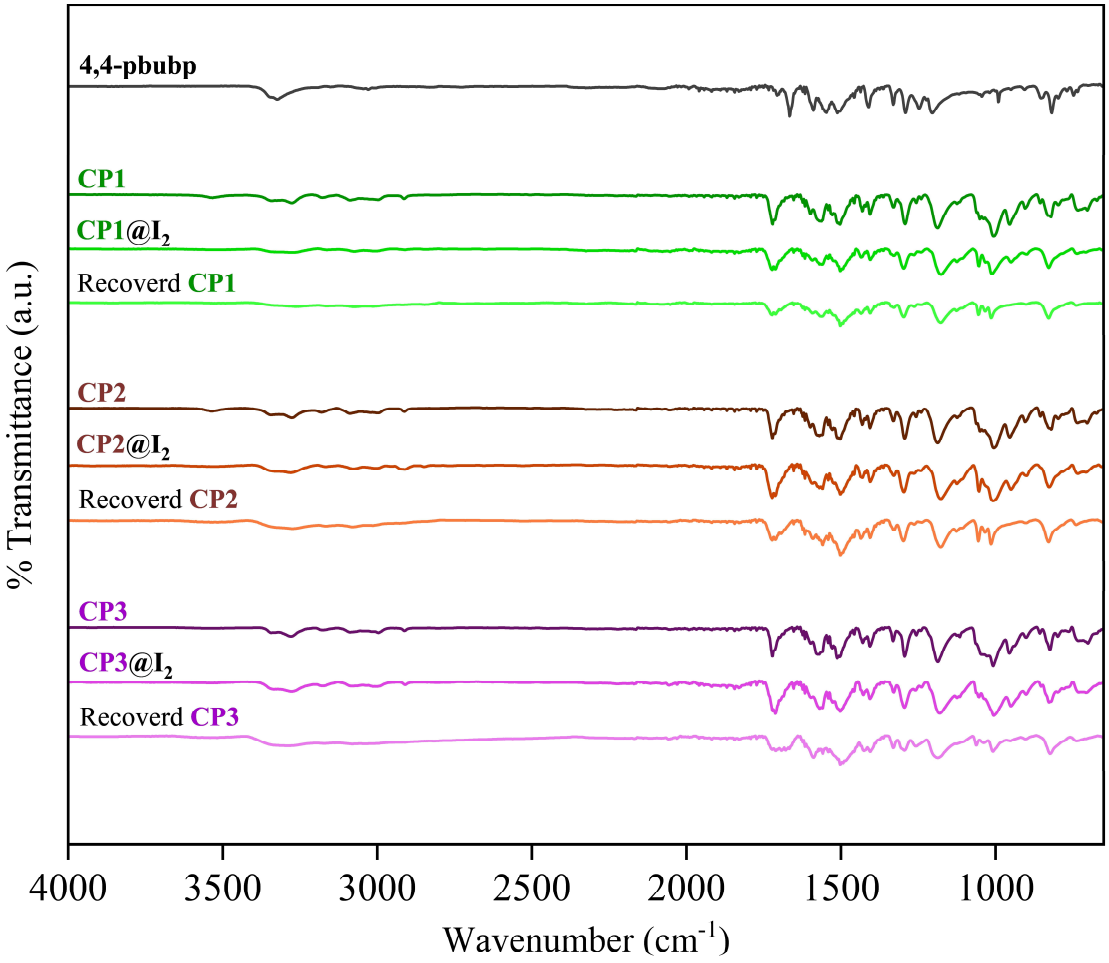

Fig. S36 ATR-FTIR spectra of **4,4-pbubp**, compounds **CP1**, **CP2** and **CP3** before and after iodine uptake.

Table S1 Selected bond lengths [Å] and angles [^{0}] for **CP1**.

Hg(1)—Cl(1)	2.3990(10)	Cl(1)—Hg(1)—N(1A)	101.24(8)
Hg(1)—Cl(2)	2.3925(12)	Cl(1)—Hg(1)—N(1B)	102.81(7)
Hg(1)—N(1A)	2.345(3)	Cl(2)—Hg(1)—N(1A)	98.59(8)
Hg(1)—N(1B)	2.309(3)	Cl(2)—Hg(1)—N(1B)	103.70(8)
Cl(1)—Hg(1)—Cl(2)	143.41(3)	N(1A)—Hg(1)—N(1B)	99.80(9)

Table S2 Selected bond lengths [Å] and angles [^{0}] for **CP2**.

Hg(1)—Br(1)	2.5228(8)	Br(1)—Hg(1)—N(1A)	102.57(10)
Hg(1)—Br(2)	2.5181(7)	Br(1)—Hg(1)—N(1B)	98.19(10)
Hg(1)—N(1A)	2.318(4)	Br(2)—Hg(1)—N(1A)	103.15(10)
Hg(1)—N(1B)	2.354(4)	Br(2)—Hg(1)—N(1B)	102.22(10)
Br(1)—Hg(1)—Br(2)	143.04(2)	N(1A)—Hg(1)—N(1B)	101.42(13)

Table S3 Selected bond lengths [Å] and angles [^{0}] for **CP3**.

Hg(1)—I(1)	2.6754(8)	I(1)—Hg(1)—N(1)	102.8(2)
Hg(1)—I(2)	2.6944(8)	I(1)—Hg(1)—N(6)$^{\#1}$	102.6(2)
Hg(1)—N(1)	2.350(7)	I(2)—Hg(1)—N(1)	99.8(2)
Hg(1)—N(1)	2.362(7)	I(2)—Hg(1)—N(6)$^{\#1}$	101.8(2)
I(1)—Hg(1)—I(2)	142.19(2)	N(1)—Hg(1)—N(6)$^{\#1}$	101.9(2)
Symmetry codes: #1: –x + 1, y + 1/2, –z + 3/2.			

Table S4 Geometry of intermolecular hydrogen bonds (D−H···A) for **CP1-CP3**.

Compound	D−H···A	d(D−H) / Å	d(H···A) / Å	d(D···A) / Å	∠ D−H···A/deg.
CP1	N2A−H2AA···O1E	0.88	1.94	2.719(9)	147
	N3A−H3AA···O1E	0.88	2.00	2.786(10)	149
	N2B−H2BA···O1D	0.88	2.03	2.836(4)	152
	N3B−H3BA···O1D	0.88	1.98	2.802(4)	156
	C1C−H1C2^{a}···O8B	0.98	2.46	3.229(4)	135
	C2C−H2C2^{a}···O8B	0.98	2.54	3.297(4)	134
	C2C−H2C1^{a}···O1C^{b}	0.98	2.48	3.446(4)	168
	C2C−H2C3^{b}···O1C^{a}	0.98	2.47	3.401(4)	159
	C1E−H1E3···Cl1^{c}	0.98	2.79	3.671	149
	C2E−H2E3···Cl1^{c}	0.98	2.80	3.678	149
Symmetry codes: *a:* x, y – 1, z *b:* –x, y – 3/2, –z + 3/2 *c:* –x + 1, y – 1/2, –z + 3/2					
CP2	N2A−H2AA···O1D	0.88	2.02	2.839(5)	154
	N3A−H3AA···O1D	0.88	1.97	2.802(6)	157
	N2B−H2BA···O1E	0.88	1.96	2.808(8)	161
	N3B−H3BA···O1E	0.88	2.08	2.903(10)	155
	C1C−H1CB^{a}···O1A	0.98	2.56	3.309(6)	133
	C2C−H2CB^{a}···O1A	0.98	2.48	3.247(6)	135
	C1C−H1CC^{a}···O1C^{b}	0.98	2.51	3.470(6)	167
	C1C−H1CA^{b}···O1C^{a}	0.98	2.50	3.413(6)	156
	C1E−H1ED···Br2^{c}	0.98	2.98	3.838	148
	C2E−H2EE···Br2^{c}	0.98	3.05	3.846	140
Symmetry codes: *a:* x, –y + 1/2, z – 1/2 *b:* –x + 2, –y, –z + 1 *c:* –x + 1, y – 1/2, – z + 1/2					
CP3	N2−H2A···O1C	0.88	2.04	2.851(11)	152
	N3−H3A···O1C	0.88	2.02	2.840(12)	155
	N4−H4A···O1A^{a}	0.88	2.01	2.835(12)	156
	N5−H5···O1A^{a}	0.88	2.07	2.873(11)	151
	C1D−H1DB^{b}···O1D^{a}	0.98	2.46	3.405(13)	162
	C1D−H1DB^{a}···O1D^{b}	0.98	2.72	3.689	171
	C1B−H1BA^{a}···O1C	0.98	2.32	3.267(14)	164
	C2D−H2DC^{b}···O2	0.98	2.44	3.255(15)	140
	C1D−H1DC^{b}···O2	0.98	2.65	3.399	133
	C1C−H1CA···O1B^{a}	0.98	2.78	3.615	144
	C2C−H2CC···O1D^{a}	0.98	2.61	3.568	165
	C1C−H2CC···I2^{c}	0.98	3.60	4.186	121
	C2C−H2CA···I2^{c}	0.98	3.86	4.440	120
Symmetry codes: *a:* x + 1, y, z *b:* –x, –y + 1, –z + 1 *c:* x , –y + 3/2, z – 1/2					

Table S5 Kinetics parameters for iodine uptake from the solution by **CP1**, **CP2** and **CP3** at room temperature.

Kinetic models	Equations	Parameters	CP1	CP2	CP3
Pseudo-first-order	$q_t = q_e(1 - e^{-k_1 t})$	Adj. R^2	0.8705	0.9861	0.8888
		q_e	132.34	150.76	61.879
		k_1	0.0352	0.0199	0.0251
Pseudo-second-order	$q_t = \frac{q_e^2 k_2 t}{(1 + q_e k_2 t)}$	Adj. R^2	0.9992	0.9966	0.9998
		q_e	199.20	181.16	108.34
		k_2	6×10^{-4}	1.7×10^{-4}	1.3×10^{-3}
Intra-particle diffusion	$q_t = x_i + k_i t^{1/2}$	Adj. R^2	0.8141	0.9400	0.7052
		k_i	8.5380	9.8599	4.5158
		x_i	90.752	21.583	52.219
Elovich	$q_t = \frac{\ln a_e b_e}{b_e} + \frac{1}{b_e}\ln t$	Adj. R^2	0.9612	0.9885	0.9127
		a	147.59	13.754	88.469
		b	0.0344	0.0280	0.0628

Table S6 Langmuir, Freundlich, and Temkin parameters of iodine removal by **CP1**, **CP2** and **CP3** at room temperature.

Models	Equations	CP1 Adj. R^2	CP2 Adj. R^2	CP3 Adj. R^2
Langmuir	$q_e = \frac{q_{max} C_e k_L}{(1 + C_e k_L)}$	0.9989	0.9872	0.9790
Freundlich	$q_e = k_F C_e^{1/n}$	0.9997	0.9893	0.9930
Temkin	$q_e = B \ln(A_t C_e)$	0.9953	0.9713	0.9784

X-ray crystallography

Diffraction data were collected at 100(1) K by the ω-scan technique, using graphite-monochromated MoK_α radiation (λ=0.71073 Å), on Rigaku XCalibur four-circle diffractometer with EOS CCD detector. The data were corrected for Lorentz-polarization as well as for absorption effects.[2] Precise unit-cell parameters were determined by a least-squares fit of the 8919 (**CP1**), 9998 (**CP2**) and 11958 (**CP3**) reflections of the highest intensity, chosen from the whole experiment. The structures were solved with SHELXT [3] and refined with the full-matrix least-squares procedure on F^2 by SHELXL.[4] All non-hydrogen atoms were refined anisotropically. Hydrogen atoms were placed in idealized positions and refined as 'riding model' with isotropic displacement parameters set at 1.2 (1.5 for CH_3) times U_{eq} of appropriate carrier atoms. In all structures, diffused electron density was found, caused probably by additional solvent molecules; the number of such molecules given in the formulae reflect the modelled molecules only. The Squeeze procedure [5] was applied in order to include this electron density in the model. In **CP1** and **CP2** one of the localized solvent DMSO molecules was refined in two alternative positions, site occupancy factors refined at 57.5(6)/42.5(6)% in **CP1** and at 50.7(12)/49.3(12)% in **CP2**.

Analysis of Hirshfeld surfaces

The surfaces are transparent to permit visualization of the asymmetric unit of each coordination polymer. The intermolecular interactions data (cf. Table S4) makes clear that the interactions discussed widely in the crystal structure section are summarized effectively in the spots. The deep red large circular depressions on each and every face of the d_{norm} surfaces indicate that they have been encapsulated in the hydrogen bond interactions. The small extent of area and light color on the surface indicates weaker and longer contact other than hydrogen bonds and the blue spots indicate the areas without close contacts. The FPs of Hirshfeld surface for compounds and relative contributions of different interactions overlapping in the full FPs are shown in Fig. S13 and S14, respectively. The Hirshfeld surfaces mapped over d_{norm} shown (as expected) that the H···H, O···H/H···O, X···H/H···X (X= Cl, Br and I) and C···H/H···C hydrogen contacts were the most outstanding interaction in the total Hirshfeld surface (Fig. S13). In all cases, the O···H/H···O interactions are highlighted by the two distinct spikes in the (d_i, d_e) region of (1.340, 1.020), (1.332, 1.022), (1.112, 0.772) C···H/H···C close contacts, which take almost 10% of the total surface (Fig. S13), can be attributed to C–H···π interaction.

References

1 P. Howlader, P. Das, E. Zangrando and P. S. Mukherjee, *J. Am. Chem. Soc.*, 2016, **138**, 1668-1676.

2 Rigaku Oxford Diffraction (2015) CrysAlis PRO (Version 1.171.38.41).

3 G. Sheldrick, *Acta Crystallographica Section A*, 2015, **71**, 3-8.

4 G. Sheldrick, *Acta Crystallographica Section C*, 2015, **71**, 3-8.

5 A. Spek, *Acta Crystallographica Section C*, 2015, **71**, 9-18.